Human interleukin-2 receptor β mutations associated with defects in immunity and peripheral tolerance

Zinan Zhang[1,2*], Florian Gothe[3,4*], Perrine Pennamen[5*], John R. James[1], David McDonald[3], Carlos P. Mata[1], Yorgo Modis[1], Anas M. Alazami[9], Meghan Acres[3], Wolfram Haller[6], Claire Bowen[6], Rainer Doffinger[7], Jan Sinclair[8], Shannon Brothers[8], Yu Zhang[2], Helen Matthews[2], Sophie Naudion[5], Fanny Pelluard[10], Huda Alajlan[9], Yasuhiro Yamazaki[11], Luigi D. Notarangelo[11], James E. D. Thaventhiran[1], Karin R. Engelhardt[3], Hamoud Al-Mousa[12], Sophie Hambleton[3#^], Caroline Rooryck[5#], Kenneth G.C. Smith[1#^], Michael J. Lenardo[2#^]

[1] Department of Medicine, University of Cambridge, Cambridge, United Kingdom
[2] Molecular Development of the Immune System Section, Laboratory of Immune System Biology and Clinical Genomics Program, National Institute of Allergy and Infectious Diseases, National Institutes of Health, Bethesda, MD, USA
[3] Institute of Cellular Medicine, Newcastle University, Newcastle, United Kingdom
[4] Dr. von Hauner Children's Hospital, Department of Pediatrics, University Hospital, Ludwig-Maximilians-Universität (LMU) Munich
[5] University of Bordeaux, MRGM INSERM U1211, CHU de Bordeaux, Service de Génétique Médicale, F-33000 Bordeaux, France
[6] Birmingham Children's Hospital, Birmingham, United Kingdom
[7] Department of Clinical Biochemistry and Immunology, Cambridge University Hospital, Cambridge, United Kingdom
[8] Starship Children's Hospital, Auckland, New Zealand
[9] Department of Genetics, King Faisal Specialist Hospital and Research Center, Riyadh, Saudi Arabia
[10] CHU Bordeaux, Department of Pathology, F-33000 Bordeaux, France
[11] Immune Deficiency Genetics Section, Laboratory of Clinical Immunology and Microbiology and Clinical Genomics program, National Institute of Allergy and Infectious Diseases, National Institutes of Health, Bethesda, MD, USA
[12] Department of Pediatrics, King Faisal Specialist Hospital and Research Center, Riyadh, Saudi Arabia

*co-first authors
#co-senior authors
^co-corresponding authors

Running Title: Human *IL2RB* deficiency

Abbreviation List:

ANA – Antinuclear antibodies
ANCA – Antineutrophil Cytoplasmic Antibodies
BFP – Blue Fluorescent Protein
CADD – Combined Annotation Dependent Depletion
FOXP3 – Forkhead Box P3
GERP – Genomic Evolutionary Rate Profiling
HSCT – Hematopoietic Stem Cell Transplant
IL-2Rβ – Interleukin-2 receptor β protein
***IL2RB* – Interleukin-2 receptor β gene**
IPEX – Immunodysregulation Polyendocrinopathy Enteropathy X-linked
MAF – Minor Allele Frequency
MD – Molecular Dynamic
NCF4 – Neutrophil Cytosolic Factor 4
NKG2C – Killer Cell Lectin Like Receptor C2 also known as KLRC2
PLZF – Promyelocytic leukemia zinc finger
SIFT – Sorting Intolerant from Tolerant
SYK – Spleen tyrosine kinase

Short Summary (36 words):

Zhang et al. identify human IL-2Rβ deficiency as a cause of severe immune dysregulation. The hypomorphic gene mutations reveal variable IL-2Rβ expression and function between different lymphocyte subsets as a means of selectively modulating immune responses.

Abstract (157 words)

Interleukin-2, which conveys essential signals for immunity, operates through a heterotrimeric receptor. Here we identify human interleukin-2 receptor (IL-2R) β chain (*IL2RB*) gene defects as a cause of life-threatening immune dysregulation. We report three homozygous mutations in the *IL2RB* gene of eight individuals from four consanguineous families that cause disease by distinct mechanisms. Nearly all patients presented with autoantibodies, hypergammaglobulinemia, bowel inflammation, dermatological abnormalities, lymphadenopathy, and cytomegalovirus disease. Patient T lymphocytes lacked surface expression of IL-2Rβ and were unable to respond to IL-2 stimulation. By contrast, natural killer cells retained partial IL-2Rβ expression and function. IL-2Rβ loss of function was recapitulated in a recombinant system, in which *IL2RB* mutations caused reduced surface expression and IL-2 binding. Stem cell transplant ameliorated clinical symptoms in one patient; forced expression of wild-type IL-2Rβ also increased the IL-2 responsiveness of patient T lymphocytes *in vitro*. Insights from these patients can inform the development of IL-2-based therapeutics for immunological diseases and cancer.

Introduction

The interleukin-2 receptor (IL-2R) complex plays a central role in control of the immune response by integrating signals from the key cytokines IL-2 and IL-15. Three distinct receptors for IL-2 are generated by combinations of three IL-2R subunits: IL-2Rα (CD25), IL-2Rβ (CD122) and IL-2Rγ (CD132) – the latter, known as the common γ chain, is also necessary for signaling by IL-4, 7, 9, 15 and 21. All three chains combine to form the high affinity IL-2R, which is constitutively expressed on $CD4^+$ regulatory T cells (T_{regs}), and induced upon activation of CD4 and CD8 T cells, B cells and some myeloid-derived subsets (Liao et al. 2013; Busse et al. 2010). A second receptor, which binds IL-15 and IL-2 with intermediate affinity, is comprised of only the IL-2Rβ and IL-2Rγ subunits; it is constitutively expressed on resting $CD8^+$ T cells and natural killer (NK) cells. The α subunit alone is a low affinity receptor. Upon ligand binding, the IL-2Rβ and IL-2Rγ subunits undergo tyrosine phosphorylation which, in turn, induces the phosphorylation of the associated Janus tyrosine kinases (JAK) 1 and 3, that phosphorylate the signal transducer and activator of transcription 5 (STAT5) transcription factor (Waldmann et al. 2006). STAT5, once dimerized and translocated to the nucleus, induces a pro-survival and proliferative transcription program. Interleukin-2 (IL-2) is primarily produced by $CD4^+$ T helper cells following T cell receptor (TCR) engagement with costimulation (Boyman et al. 2012). It potently stimulates T cell proliferation, differentiation (promoting Th1, Th2, and Th9, and suppressing Th17 polarization) and cytolytic effector activity. It also plays a key role in peripheral tolerance by promoting the generation and maintenance of regulatory T cells (T_{reg}) and antigen-specific peripheral T cell clonal deletion (Hatakeyama et al. 1989; Takeshita et al 1992; Lenardo, 1991). CD25 deficient mice demonstrate grossly normal early B and T cell development, but lymphadenopathy and impaired T cell activation and clonal deletion. As they age, these mice develop autoimmune and inflammatory disease (e.g. hemolytic anemia and inflammatory enteropathy) (Willerford et al. 1995). Humans with CD25 deficiency have a similar phenotype, developing prominent autoimmune disease with less consistent evidence of immunodeficiency, and resembling patients with IPEX, due to FOXP3 deficiency, thus indicating the impact of loss of the high-affinity IL-2 receptor can be ascribed to a loss of peripheral tolerance (Scharfe et al. 1997, Caudy et al. 2007).

The role in immunity of IL-2Rβ is less well understood, and no monogenic cause of human IL-2Rβ deficiency has yet been described. Although a case of NK-SCID was previously reported, in which the patient did not express IL-2Rβ, no mutation within *IL2RB* was identified (Gilmour et al. 2001). IL-2Rβ-deficient mice had severe autoimmunity and diminished cytolytic effector function, with splenomegaly, lymphadenopathy, elevated IgG1 and IgE levels, and ANA and anti-dsDNA autoantibodies (Suzuki et al. 1995). They succumbed to autoimmunity around 12 weeks unless rescued by the adoptive transfer of T_{regs} (Malek et al. 2002). Despite showing evidence of activation, e.g. increased CD69, the T cells of IL-2Rβ-deficient mice failed to respond to stimuli including IL-2, PMA, and ionomycin, and had diminished $CD8^+$ T cell cytolytic activity when re-challenged (Suzuki et al. 1995). This, plus the observation that they have reduced NK cell numbers (Suzuki et al. 1997), implies that IL-2Rβ deficiency in mice could produce susceptibility to infection in addition to T cell activation and autoimmunity. IL-2Rβ-mediated signaling is implicated in pathways known to be important in human autoimmune disease, and loci containing it have been associated with asthma and juvenile-onset arthritis in genome-wide association studies (Moffatt et al. 2010, Hinks et al. 2013). Moreover, high-dose

IL-2 therapy is approved for use in renal cell carcinoma and malignant melanoma and encouraging early phase studies of low-dose IL-2 in Type-1 diabetes, graft-versus-host disease and systemic lupus erythematosus have led to over 14 on-going phase 2 and 3 trials (Ahmadzadeh et al. 2006; Ye et al. 2018). It will thus be important to understand the biology of IL-2Rβ, and the impact of IL-2Rβ deficiency, in humans. To this end, we describe human homozygous recessive IL-2Rβ deficiency in four consanguineous families with 8 affected individuals, which was associated with autoimmunity and immunodeficiency.

Results

Clinical phenotype and genotype of patients in a combined immunodeficiency/autoimmunity cohort.

We investigated the medical records and clinical data of eight affected individuals from four consanguineous families with South Asian, Middle Eastern, and Eastern European origins, residing in countries on three different continents. All the patients have a history of severe immunodeficiency and autoimmunity (Figure 1 and Supplementary Table 1). Kindred A includes a six-year-old boy (A1) and his three-year-old sister (A2) born to first cousin Pakistani parents (Figure 1A). A1 was initially hospitalized at the age of two for thyrotoxicosis secondary to Graves' disease and A2 was hospitalized at the age of six months for failure to thrive and persistent diarrhea (Supplementary Table 1). Since their initial hospital course, A1 has developed severe gastroenteritis and dermatitis and A2 has had pulmonary, gastrointestinal, and urinary infections as well as ANCA+ vasculitis. Patient A1 has improved with rituximab treatment but continues to be intermittently ill. Patient A2 received an allogeneic hematopoietic stem cell transplant (HSCT) and has recovered with no sequelae. Kindred B consists of a girl (B1) born to related parents of South Asian origin. B1 initially presented in a collapsed state with severe diarrhea at the age of 4 weeks and was found to have enteropathy, dermatitis, and later CMV viremia with hepatitis. She improved with immunosuppression and antiviral therapy but ultimately succumbed to probable CMV pneumonitis and respiratory failure after HSCT. Kindred C includes a boy (C1) and his first female cousin (C2) born to consanguineous Saudi Arabian parents. C1 presented with suppurative ear infections at the age of 6 months. C2 presented with chest and ear infections and diarrhea at the age of 2 months. Subsequently, both suffered recurrent otitis, severe dermatitis, CMV viremia and food allergies. C1 and C2 died from probable CMV pneumonitis at the age of 3 years old and 18 months old, respectively.

Kindred D consists of two fetuses (D1, D3) and a premature female neonate (D2) conceived by a Romany family living in France. D1, D2, and D3 were found to have intra-uterine growth retardation and reduced fetal movement; skin-like floating membranes were also present in the amniotic fluid in all three cases. While it was not possible to evaluate the fetuses for immunodeficiency, autoimmune skin desquamation in utero is consistent with echogenic debris findings in prenatal IPEX patients (Louie et al. 2017). D2 was delivered pre-maturely by emergency Cesarean section at 31 weeks' gestation, but she died two hours later of respiratory failure. D1 and D3 pregnancies were terminated due to fetal abnormalities at 25 weeks and 30 weeks, respectively. In summary, all the patients who had survived the neonatal period had recurrent infections, as well as autoimmune disease, leading to early death in most cases.

Immune dysregulation was a key shared feature across these four kindreds, manifest as enteropathy, dermatitis, autoimmune hemolytic anemia, and hypergammaglobulinemia (Figure 1). All the children with IL-2Rβ deficiency also had recurrent infections, including defective handling of herpesviruses (CMV or EBV viremia in all; CMV disease in 4 of 5; Supplementary Table 1). Chest radiographs of patient A2 revealed a pleural effusion and numerous small pulmonary nodules and tree-in-bud opacities suggestive of CMV pneumonia in the context of CMV viremia (Figure 1B). CT imaging also revealed hepatosplenomegaly and marked lymphadenopathy in A2 (Figure 1B); a clinical feature that was noted in all five patients.

Skin abnormalities are a key hallmark of this disease. A1, A2, B1, C1, and C2 all had severe dermatitis and D1, D2, and D3 had patches of hyperkeratosis and significant infiltration of B and T lymphocytes on skin immunohistochemistry (Figure 1C). Four out of the five children have also had severe diarrhea and infectious/autoimmune enteropathy. Endoscopy of patient B1 showed villous atrophy and gastrointestinal biopsies revealed chronic inflammatory infiltration of the duodenum and rectum (Figure 1D). Additional hallmarks of disease include: autoimmune hemolytic anemia (4/5 patients) and hypergammaglobulinemia (5/5 patients) comprising predominantly class-switched isotypes: IgA, IgG, and IgE (Figure 1E and Supplementary Table 2). Overall, CD4 cell numbers were normal but two of the patients had low CD8 T cell counts, while NK numbers were increased (Supplementary Table 2). T cell proliferative responses measured in B1 were also globally impaired (Supplementary Figure S1).

Identification of protein-coding mutations in the gene encoding IL-2Rβ (CD122)

Because of the early onset of disease in consanguineous families, we sought a genetic cause by whole exome DNA sequence analysis of the 4 kindreds. We identified three different *IL2RB* gene mutations (Figure 2A). For Kindreds A and B, the *IL2RB* chr22: g.37538526 A>G (p.Leu77Pro) missense variant was prioritized. The mutation occurs in exon 4 (out of 10) and is not found in dbSNP, ESP, or ExAC databases, but has a minor allele frequency (MAF) of 0.00001218 in gnomAD. The p.Leu77Pro mutation introduces a restrictive proline-proline motif in the extracellular D1 domain of IL-2Rβ (Figure 2B). For Kindred C, the g.37539634 C>T (p.Ser40Leu) missense variant was prioritized and not found in any databases of genomic variation. The mutation appears to be located at the interface of IL-2Rβ and IL-2 (Figure 2B). For Kindred D, a g.37537259 G>A (p.Gln96*) stop-gain mutation was identified and also not found in any databases. This mutation would lead to significant truncation of the 552 amino acid protein. Due to the predicted deleterious nature of these variants, their segregation with disease and the similarity in phenotype with a mouse knock-out model, IL2RB represented an attractive candidate disease gene. Other prioritization criteria that were taken into consideration include: Combined Annotation Dependent Depletion (CADD) score, quality of reads, Genomic Evolutionary Rate Profiling (GERP) conservation score, co-segregation of alleles, sorting intolerant from tolerant (SIFT) score, polymorphism phenotyping (PolyPhen2) score, tissue specific expression levels, structural modeling, and primary literature reviews leading to the conclusion that these variants were likely responsible for the disease. Other rare variants that were candidate disease alleles in individual families are listed in Supplementary Table 3; the deleterious IL-2RB alleles were the only variants that correlated with disease in all families.

The L77P IL-2Rβ missense mutation causes loss of surface expression and function in T cells

At baseline, IL-2Rβ is normally highly expressed on the surface of NK cells and to a lesser extent on T cells; however, patients with the L77P mutation have markedly decreased surface expression of IL-2Rβ on NKs, CD4 T cells, and CD8 T cells as assessed by flow cytometry (Figure 2C-D). A healthy heterozygous parent showed intermediate surface expression of IL-2Rβ (Figure 2D). Despite diminished cell surface IL-2Rβ expression, immunoblotting of cytosolic lysates of patient NKs, CD4 T, and CD8 T cells revealed strikingly

more IL-2Rβ than healthy controls (Figure 2E-G). This implied that the mutant L77P IL-2Rβ protein was sequestered intracellularly due to misfolding and an inability to properly traffic to the cell surface for subsequent turnover. In keeping with this hypothesis, the faster migration of L77P IL-2Rβ protein relative to WT IL-2Rβ is likely due to incomplete glycosylation branching modifications that are added post-translationally outside the endoplasmic reticulum (ER) (Figure 2E). In addition, the affected neonate (D1) and fetuses (D2, D3) from Kindred D with the more severe p.Q96* stop gain mutation, resulting in a significant truncation, had no IL-2Rβ protein expression (Figure 2H).

Reduced signaling by mutant IL-2Rβ proteins encoded by patient alleles

We reconstituted the IL-2R complex in HEK293T cells via transfection of expression plasmids encoding IL-2Rβ, and IL-2Rγ, JAK-3, and STAT5; this system can transduce a signal from IL-2 to intracellular mediators such as the STAT signaling proteins (John et al. 1999; Majri et al. 2017). We used this system to compare the protein-coding sequences of the wild-type or L77P mutant IL-2Rβ and GFP (separated by a P2A sequence) under the control of a tetracycline (Tet) -inducible promoter. As expected, cells transfected with the wild-type plasmid showed increasing IL-2Rβ surface expression that correlated with increasing GFP expression after Tet induction (Figure 3A). However, cells transfected with the mutIL2RB plasmid showed very low surface IL-2Rβ expression, except at very high levels as judged by GFP co-expression (Figure 3A). Given similar levels of expression of the BFP control for tetracycline-inducible system and GFP expression, wild-type IL-2Rβ is expressed at much greater abundance on the cell surface than the L77P mutant (Figure 3B). As observed in the L77P mutant patient lymphocytes, there is an increase in total cytoplasmic IL-2Rβ protein, despite decreased surface expression, in cells transfected with the mutant (Figure 3C). Confocal imaging of the live HEK293T cells transfected with an ER marker (KDEL-BFP) and wtIL-2RB-GFP or mutIL-2RB-GFP showed that mutIL-2RB-GFP co-localized with KDEL-BFP and therefore was being sequestered in the ER (Figure 3D), as we hypothesized from the patient data. Together these experiments demonstrate that even when the L77P IL-2Rβ is reconstituted in an exogenous HEK293T cell line, the allele encodes a mutant protein that is sequestered in the ER and inefficiently reaches the cell surface, thus recapitulating the patients' cellular phenotype.

Using our reconstituted receptor system, we also compared the Q96* and S40L alleles to the L77P allele for IL-2Rβ surface expression and phosphorylation of STAT5 (pSTAT5) after IL-2 stimulation (Figure 3E-F). As expected, the Q96* allele, which encodes an early stop codon and truncation of IL-2Rβ prior to the transmembrane domain, generated no IL-2Rβ surface expression and showed no pSTAT5 response to IL-2 stimulation (Figure 3E-F). The low level of L77P expressed at the cell surface was nonetheless capable of supporting some phosphorylation of STAT5 in response to IL-2, indicating hypomorphic behavior of this allele. By contrast, the S40L IL2RB allele promoted IL-2Rβ surface expression but conferred no response to IL-2 stimulation (Figure 3E-F). Molecular modelling of the S40L mutant showed that the substitution introduces steric clashes with main chain atoms in the BC2 loop (residues 157-165) in the D2 domain, which we predict would disrupt the IL-2 binding interface of IL-2Rβ (Figure 3G), consistent with this variant's lack of responsiveness to IL-2 (Figure 3F). In addition, we performed molecular dynamics (MD) simulations on WT IL-2Rβ and the L77P and S40L

mutants. After 100 ns of simulation, residues 76-78 in the L77P mutant adopt a different backbone conformation and do not contribute a β-strand to one of the β-sheets in the D1 domain as in WT (Supplementary Figure S2), which is consistent with our functional evidence that the L77P mutant is misfolded and sequestered in the ER. In an MD simulation of the S40L mutant, the BC2 loop and specifically key IL-2 binding residues His159 and Tyr160 adopted a conformation that would clash with an IL-2 molecule bound in the same position as in the wild type complex. The D1 domains also rotated relative to the D2 domain in the S40L mutant by approximately 15˚, altering the shape of the IL-2 binding surface (Figure 3G). As predicted by the MD simulation, the S40L mutant had significantly decreased affinity to IL-2 - comparable to levels in the negative control without IL-2Rβ based on a biotinylated cytokine-streptavidin fluorophore flow cytometry assay (Figure 3H). Thus, by using this reconstituted system, we define three distinct mechanisms in humans for IL-2Rβ deficiency by showing that it can occur due to an absence of IL-2Rβ (Q96*), impaired surface expression (L77P), and decreased binding of IL-2 (S40L).

*Patient T cells show impaired IL-2R*β*-dependent signaling*

We next explored the impact of *IL2RB* mutations on interleukin signaling in patient T lymphocytes by measuring STAT3 and STAT5 phosphorylation after interleukin stimulation (Figure 4). High dose IL-2 normally triggers tyrosine phosphorylation of the cytoplasmic tails of the IL-2Rβ and IL-2Rγ and downstream STAT1, STAT3, and STAT5 phosphorylation via the JAK1 and JAK3 Janus kinases. Consistent with a loss of function phenotype, we found that $CD4^+$ and $CD8^+$ T cells, which were available for laboratory analysis from patients A1 and B1, failed to phosphorylate STAT5 in response to IL-2 or IL-15 stimulation whereas robust phosphorylation was observed in cells from healthy controls (Figure 4A-E). By contrast, patient T cells were fully responsive to IL-7 stimulation, indicating that the defect of IL-2Rβ-dependent signaling was selective (Figure 4E). Interestingly, $CD4^+$ T cells from A0, the father with a heterozygous L77P genotype, have enough surface expression of IL2-Rβ to phosphorylate STAT3 and STAT5 at a comparable level to healthy controls (Figures 4A and B) although there was a trend towards reduced STAT3 and STAT5 phosphorylation in heterozygous $CD8^+$ T cells (Figures 4C and D). Thus, surface IL-2Rβ deficiency impairs downstream STAT phosphorylation in response to IL-2 and IL-15 stimulation in a cell-type- and receptor expression-dependent manner.

In keeping with current understanding of the critical role of IL-2 signaling in the maintenance of regulatory T (T_{reg}) cells in the periphery, the $CD25^{hi}FoxP3^+$ $CD4^+$ T cell compartment was almost empty (Figure 4F). Consistent with the inability of peripheral T cells to utilize and consume IL-2 and IL-15, the patients had elevated levels of serum IL-2 and IL-15 and their T cells did not upregulate CD25 expression when stimulated with the same cytokines (Figure 4G and 4H). Taken together, the profound reduction of STAT5 signalling within the $CD4^+$ T cell compartment, inability to upregulate CD25, and the absence of $CD25^{hi}FOXP3^+$ T_{reg}s closely mirrors the situation in IL2RB-knock out mice and other known disorders of Tregs such as monogenic deficiencies of FOXP3 and CD25. Therefore, this could explain at least in part the various autoimmune manifestations we observed early in life.

Hypomorphic nature of L77P IL2RB mutation in NK cells

The NK compartment of IL2RB-knockout mice is almost completely depleted, but our patients bearing hypomorphic mutations instead showed an expansion of NK cells (Supplementary Table 2) and an increase in $CD56^{bright}$ relative to $CD56^{dim}$ NKs (Figure 5A) (Suzuki et al. 1995). These unusually abundant $CD56^{bright}$ NK cells expressed abnormally high levels of the cytotoxic effector proteins perforin and granzyme B (Figure 5B). A similar increase of the human $CD56^{bright}$ NK cell compartment has been observed in patients experiencing chronic cytokine exposure through low dose IL-2 therapy (Ito et al, 2014), CD25 blockade (Bielekova et al, 2006) or low dose IL-15 treatment (Dubois 2017), associated with increased *ex vivo* cytotoxic function. Indeed, residual expression of $IL\text{-}2R\beta^{L77P}$ was clearly detectable (Figure 2C and 2D), just as it had been on the surface of transfected 293T cells. Moreover, this residual IL-2Rβ expression could sustain IL-2 and IL-15 signal transduction and downstream STAT5 phosphorylation (Figure 5C).

We were able to examine NK cell effector function systematically in patient B1. When provided with the target cell line K562, patient NK cells degranulated to a similar extent to control NK cells, with evidence of priming by both IL-2 and IL-15 (Figure 5D and S3B). Moreover, cytotoxicity towards K562 was increased in patient NK cells compared to control with IL-2 or IL-15 priming (Figure 5E). However, patient NK cells were poor producers of IFN in response to the same cytokines (Figure 5F and S3C). This effect was IL2Rβ-dependent, because the same cells could produce normal levels of IFNγ when stimulated with IL-12. These data support the conclusion that L77P is a hypomorphic mutation of IL-2Rβ that all but abolishes IL-2 signaling in T cells but still transduces residual signaling in high IL-2R-expressing cell subsets like NK cells. As a result, NK cells persist and can respond to the IL-2 and IL-15 that we speculate are normally produced but not consumed by IL-2Rβ-deficient T cells. Our data show that various outcomes of IL-2Rβ signaling are differentially affected by the L77P variant – from absent (IFNγ production, Figure 5F and S3C) to reduced (CD25 upregulation, Figure 4H and S3A) to supra-normal (cytotoxicity, Figure 5E)**; however, these findings are based only on a single patient and firm conclusions are difficult due to donor variability.**

With this evidence of altered NK phenotype in mind, we hypothesized that NK differentiation might be perturbed in other ways. In particular, the NK compartment is known to adapt to the presence of CMV by expansion of memory-like cells that co-express NKG2C and CD57 on their surface (Lopez-Verges et al, 2010). Such cells were strikingly absent from both A1 and B1 (Figure 5G and 5H), even though an $NKG2C^{+}$ population was present, suggesting CMV recognition. To explore whether there was a general problem with NK maturation, we examined the expression of the transcription factor PLZF and its downstream targets SYK and FcεRIγ (Lee et al., 2015 and Schlums et al., 2015). This analysis confirmed a failure of patient $NKG2C^{+}$ NK cells to complete their differentiation by downregulating PLZF, SYK, and FcεRIγ, as well as upregulating CD57 (Figure 5I and 5J). We conclude that the NK compartment and its response to CMV is systematically altered in the context of the hypomorphic IL2RB mutation. We suggest that this is at least in part responsible for the observed clinical susceptibility to CMV disease.

Lentiviral rescue of IL2RB and STAT phosphorylation in patient T cells

Finally, we performed complementation by lentiviral transduction of patient T cells with wild-type IL-2Rβ (Figure 6). Patient T cells were activated with anti-CD3 and anti-CD28 beads, transduced with lentiviral WT-IL2RB and GFP, and cultured in the presence of IL-7 rather than IL-2. Patient $CD3^+$ T cells were transduced with greater than 50% transfection efficiency (Figure 6A) and expressed high levels of IL-2Rβ on the cell surface (Figure 6B). While patient T cells that were not transduced with WT-IL2RB failed to respond to high dose IL-2 stimulation as expected, transduced patient T cells, when stimulated with IL-2, were able to phosphorylate STAT3 and STAT5 (Figure 6C and 6D). Transduction of WT-IL2RB did not restore IL-2 response back to control levels (Figure 6E), but this may be due to heterodimerization of L77P IL-2Rβ and WT IL-2Rβ leading to partial ER sequestration of the WT chain (Pillet et al., 2008). Nonetheless, lentiviral transduction of WT-IL2RB partially rescues STAT phosphorylation in response to IL-2 in patient T cells indicating that the failure of IL-2 response in this patient is due to the genetic abnormality of IL2RB

Discussion

Here we provide the first report of autosomal recessive IL-2Rβ deficiency in four pedigrees harboring five affected liveborn children with immunodeficiency and autoimmune disease and three perinatally affected fatalities. Clinical hallmarks of the disease include prominent immune dysregulatory phenomena such as enteropathy, skin abnormalities, autoimmune hemolytic anemia, and hypergammaglobulinemia, together with susceptibility to respiratory and herpesvirus infections. We demonstrate that the three mutant alleles cause IL-2Rβ deficiency by different biochemical mechanisms. Kindreds A and B have the hypomorphic L77P IL-2Rβ mutation which interferes with egress from the endoplasmic reticulum. We discovered that this abrogates surface expression and IL-2 signaling in T cells, but that NKs not only retain modest surface expression and responsiveness to IL-2 but quite potent cytolytic activity. Kindred C possesses the S40L IL-2Rβ mutant, which has decreased responsiveness to IL-2 despite being expressed on the cell surface. Our analysis shows that this is due to an amino acid side group clash in the receptor: ligand interaction site. This mutation may also be hypomorphic in nature given IL-2Rβ expression, but studies to characterize this were limited by sample availability. Kindred D has the most severe Q96* IL-2Rβ stop gain mutation. The severity of this mutation is reflected not only in the perinatal phenotype in the neonate and fetuses but also by the complete absence of IL-2Rβ expression and IL-2 signaling. However it cannot be excluded that the severe phenotype in Kindred D may be due to the added effects of other genetic variants. A NCF4 variant also co-segregated in the kindred but the specific variant is reported in ClinVar to be likely benign and is not very rare, with a MAF > 0.001. Despite the differences in mechanism, all the mutations cause IL-2Rβ dysfunction in some manner and lead to a similar constellation of clinical features.

Specifically, the hypomorphic L77P IL-2Rβ mutation highlights the significance of variable IL-2Rβ expression in different lymphocyte subsets as a means of modulating immune function. The L77P mutation causes ER sequestration and thus minimal IL-2Rβ surface expression in patient lymphocytes despite increased total IL-2Rβ protein. This decreased IL-2Rβ surface expression prevents downstream STAT3 and STAT5 phosphorylation following IL-2 stimulation in T cells. By contrast, NK cells are still capable of responding to IL-2 and maintain normal cytotoxic function, likely due to the cell's intrinsic high expression of IL-2R. Nonetheless, abnormalities of NK adaptation to CMV and IFNγ production may contribute to the viral susceptibility observed in most patients.

While the human IL-2RB deficiency shares many similarities with the IL2RB knockout (KO) mouse and FOXP3-deficient IPEX patients, there are interesting key differences. Like the knockout mouse (Suzuki et al. 1995), the IL-2RB deficient patients have autoimmune hemolytic anemia, elevated autoantibodies, and hypergammaglobulinemia (IgG and IgE), lymphadenopathy, and splenomegaly. In vitro both the IL-2RB KO mouse and IL-2RB deficient human T cells proliferate poorly in response to IL-2 and TCR stimulation. Human IL-2RB disease reveals that deficient IL-2RB also leads to skin abnormalities and enteropathy, which is not seen in the KO mouse. In addition, in the human patients, we observed an expansion of NK cells and skewing of the NK compartment, while a reduction of NK cells was recorded in the KO mouse (Suzuki et al. 1997). These observations might reflect the hypomorphic nature of the human disease alleles compared with complete loss of function in the mouse model and/or

differences in the role of IL-2/15Rβ in NK maturation in the two species (Renoux et al. 2015). Mirroring the KO mouse, the IL-2Rβ deficient patients also lack $CD25^+$ $FoxP3^+$ regulatory T cells, thus explaining the overlap in clinical features of immune dysregulation with IPEX syndrome. Enteropathy, dermatitis, and hemolytic anemia were seen in both disorders, although only one IL-2RB patient (A1) presented with any endocrinopathy – a hallmark of IPEX. A distinctive component of IL-2RB deficiency is the presence of beta-herpesviral disease in addition to severe autoimmune/inflammatory disease. This combination recalls CD25 deficiency, where beta-herpesviral susceptibility has also been noted (Scharfe et al. 1997, Caudy et al. 2007). The presence of both immunodeficiency and autoimmune/inflammatory disease as defining features of IL-2RB and CD25 deficiency states is consistent with the multi-faceted role of IL-2 signaling biology in the immune system.

The current definitive treatment for IL-2Rβ deficiency is hematopoietic stem cell transplant. Patient A2 received an allogeneic HSCT and has had complete resolution of her symptoms. However, there are high risks associated with HSCT, as exemplified by patient B1, and the hope is that understanding the pathophysiological mechanism of IL-2Rβ deficiency can guide the development of novel therapeutics. One approach might be to re-purpose IL-2 anti-IL-2 antibody complexes (Boyman et al. 2006), IL-2 superkine (Levin et al. 2012), ortho-IL2 analogs (Sockolosky et al. 2018), or IL-2 Fc fusion proteins (Vazquez-Lombardi et al. 2017) as a potential means of hyper-stimulating residual surface IL-2Rβ. Monoclonal anti-human IL-2 antibody MAB602 (mouse S4B6) in complex with IL-2 was found to selectively promote proliferation of effector T cells, while the antibody clone 5344 (mouse JES61) induced proliferation of T_{regs} (Boyman et al. 2006). Similarly, the H9 IL-2 superkine was engineered to have enhanced binding to IL-2Rβ independent of CD25 (Levin et al. 2012). Another approach to hyper-stimulating the IL-2Rβ mutant would be to develop an orthoIL-2 with specific binding to the mutant (Sockolosky et al. 2018). The fact that we find hypomorphic mutations in the liveborn children suggests that an approach involving hyper-stimulating the IL-2 axis may ameliorate disease.

In summary, our identification of human IL-2Rβ deficiency as a monogenic cause of immunodeficiency and autoimmunity provides insight into one of the principal signaling pathways of the immune activation and peripheral tolerance and should prompt prenatal screening of IL-2RB mutations and genetic counseling in families at risk.

Acknowledgments

This work was supported by the Wellcome Trust (Investigator Award 083650/Z/07/Z to KGCS, 207556/Z/17/Z to SH, 101908/Z/13/Z to YM, 099966/Z/12/Z to JRJ), the Division of Intramural Research, National Institute of Allergy and Infectious Diseases, NIH, Merck, Inc, and the UK National Institute of Health Research Cambridge Biomedical Research Centre and the Sir Jules Thorn Charitable Trust (12/JTA to SH). Z.Z. was supported by the NIH-Oxford-Cambridge Scholarship in Biomedical Research program and the NIH M.D./Ph.D partnership program with Harvard Medical School. F.G. was supported by the Deutsche Forschungsgemeinschaft (GO2955/1-1).

The authors thank John Sowerby, Iosifina Foskolou, Lixin Zheng, Francesco Colucci, Morgan Similuk, Warren Leonard, and Helen Su for their advice and insight. We thank Daniil Prigozhin for advice on molecular dynamics simulations and Danny Lim for blood processing at Hematology LabPlus at Auckland City Hospital. We thank the Genomics Core Facility, Newcastle University and Patricia Fergelot at the Genome Transcriptome Facility of Bordeaux BIOGECO, INRA for their support in whole exome sequencing. We acknowledge the Cambridge Institute of Medical Research (CIMR) and Newcastle University Flow Cytometry Core Facility (FCCF) for assistance with the generation of Flow Cytometry data. Finally, we thank all the patients described in this manuscript and their families for facilitating this work.

The authors declare no competing financial interests.

Author contributions: Z. Z. and F.G. performed the majority of the experiments and analyses. Z.Z., F.G., S.H., C.R., K.G.C.S., and M.J.L. conceived and planned the experiments. J.E.D.T, K.R.E., H.A-M., S.H., C.R., K.G.C.S., and M.J.L. supervised the project. Z.Z., F.G., S.H., K.G.C.S., and M.J.L. wrote the manuscript. All authors discussed and revised the manuscript. P.P. and Z.Z. performed in vitro experiments on Kindred D samples. J.R.J. assisted with imaging and reconstitution studies. D.M. assisted with flow cytometry studies. C.P.M. and Y.M. performed molecular dynamic simulations. A.M.A., H.A., and Z.Z. performed reconstitution experiments involving the S40L mutation. M.A., R.D., S.N., F.P., and Y.Y. assisted with experiments. Y.Z. performed the initial genomic analyses. W.H., C.B., J.S., S.B., H.M., and L.D.N. referred patients, provided clinical data, and coordinated sample collection.

Methods

Human Subjects
Written informed consent was provided by all human subjects or their legal guardians in accordance with the 1975 Helsinki principles for enrollment in research protocols that were approved by the Institutional Review Board of the National Institute of Allergy and Infectious Diseases, National Institutes of Health and the Newcastle and North Tyneside Research Ethics Committee 1, UK. Patient and healthy control blood was obtained at Starship Children's Hospital in Auckland, New Zealand, Addenbrooke's Hospital in Cambridge, United Kingdom, and Great North Children's Hospital in Newcastle, United Kingdom under approved protocols.

Genetic Analysis
DNA was obtained from probands and family members by isolation and purification from peripheral blood mononuclear cells (PBMCs) using Qiagen's DNeasy Blood and Tissue Kit. The DNA was then submitted for whole exome sequencing (WES) by Illumina sequencers in the United States, United Kingdom, France, and Saudi Arabia. The reads were filtered for sequence quality and then mapped on to the h19 human genome reference by Burrows-Wheeler Aligner with default parameters. Alignment, variant calling, and annotation were performed by the in-house bioinformatics core using the Genome Analysis Toolkit version 3.4 (Broad Institute) and GEMINI (GEnome MINIng). The IL2RB variant was confirmed by Sanger sequencing of PCR amplification products of cDNA, generated by reverse transcription of RNA using SuperScript IV VILO kit (Thermo) and the following PCR primers: F-CCTGTGTCTGGAGCCAAGAT and R-GGGTGACGATGTCAACTGTG (Sigma Aldrich) or F-CCTCACAGTGGTTGGCACA and R-GCACTCTCTCCCTGGGTG (Sigma Aldrich).

Cells and Media
Primary patient or control PBMCs were obtained from whole blood subjected to Histopaque/Ficoll density gradient separation. The PBMCs were then washed with PBS and frozen in complete RPMI with 10% DMSO in liquid nitrogen for later use or -80°C for transport. HEK293T and K562 cells were obtained from the European Collection of Authenticated Cell Cultures and tested mycoplasma-free (ECACC). Human cells were cultured in RPMI (Sigma Aldrich) or DMEM (Sigma Aldrich) supplemented with 10% heat-inactivated fetal bovine serum (Sigma Aldrich), 1% penicillin/streptomycin (Gibco), and 1% Glutamax (Gibco). Recombinant human IL-2, IL-7, and IL-15 (Peprotech) was used for stimulation. XVIVO 15 media (Lonza) supplemented with 1-10% human AB serum (Sigma Aldrich) was used for STAT phosphorylation assays.

Antibodies
The following monoclonal primary rabbit anti-human antibodies from Cell Signaling Technologies (CST) were used for Western blot analysis: anti-IL2RB, anti-GFP, anti-vinculin, and anti-IL2RA. Rabbit anti-beta actin (Abcam) and goat anti-IL2RG (Thermo Fisher Scientific) were also used. Secondary HRP-linked anti-rabbit IgG and anti-goat IgG antibodies (CST) were used to conjugate to the respective primary antibodies. The following flow cytometry antibodies are from Biolegend: CD3-AF700, CD3-PerCp-Cy5.5, CD3-BV705, CD4-Pacific Blue, CD56-PE-Cy7, CD122-PE-Dazzle, CD132-APC, CD25-APC-Cy7, CXCR5-FITC, CD45RA-PerCp-Cy5.5, CD127-APC, HLA-DR-Pacific Blue, and Live/Dead-Zombie Aqua, pSTAT3-AF647,

CD20 (2H7), PD-1 (EH12.2H7), CD45RA (HI100), CD127 (A019D5), TNFα (MAB11), CD56 (5.1H11), CD56 (HCD56), CD16 (3G8), CD19 (HIB19), CD122 (TU27), CD57 (QA17A04), Syk (4D10.2) and Perforin (dG9); Thermo Fisher Scientific: CD4-APC-eF780, CD56-APC-eF780, TCRγδ (B1.1), and TCRVα24Jα18 (6B11); BD Bioscience: CD25-PE, pSTAT5-AF488, CD4 (SK3), CD3 (UCHT1), CD8 (RPA-T8), CD25 (2A3 or M-A251), CCR7 (3D12), CD45RO (UCHL1), Granzyme B (GB11), IFN-γ (B27), STAT5 (47/Stat5), S6 (N7-548), FoxP3 (259D/C7), CD127 (HIL-7R-M21), CD56 (NCAM16.2), CD28 (CD28.2), CD95 (DX2), CD16 (3G8), CD107a (H4A3), CD69 (FN50), IL-2 (5344.111) and PLZF (R17-809); Miltenyi: CD132 (REA313); Merck: FcεRIγ (polyclonal) and R&D Systems: NKG2C (134591). Cell trace violet (Thermo Fisher Scientific, MA, USA) was used to label K562 cells. Cell viability was assessed using Zombie aqua or NIR, 7-AAD (all from Biolegend, CA, USA) or LIVE/DEAD Fixable Green (Invitrogen, Thermo Fisher Scientific, MA, USA).

Flow Cytometry

Cells were pelleted by centrifugation and stained with antibodies in FACS Buffer (1-2% FBS, 0.05% sodium azide, and 2-5 mM EDTA in PBS) at 4°C for 30-60 minutes. The stained cells were then washed with PBS or FACS buffer, pelleted, and resuspended at ~1x10^6 cells/ml in FACS Fix Buffer (FACS Buffer with or without 1% PFA) for flow cytometry analysis (Fortessa, Symphony A5, or FACS Aria Fusion systems). The flow data was analyzed using FlowJo or Treestar.

Western Blot

Cells were lysed with NuPage LDS sample buffer (Thermo Fisher Scientific) at the concentration of 10^5 cells per 15uL LDS supplemented with 10% BME and Benzonase Nuclease (Sigma Aldrich). The samples were then denatured at 70°C. Protein lysates were separated by SDS-PAGE on 4-12% Bis-Tris precase gels (Invitrogen) and transferred to a PVDF membrane (Invitrogen) by iBlot (Thermo Fisher Scientific) or wet transfer. Membranes were then blocked in milk with 5% Tris-buffered saline with 0.01% Tween-20) TBST for an hour at room temperature and then incubated with primary antibody in milk or 5% BSA overnight at 4°C. The membrane was washed for 3 x 10 minutes with TBST at room temperature and then stained with HRP-linked secondary antibody in milk for 1 hour at room temperature. After 3 x 10 minute washes with TBST and 1 x 10 minute wash with PBS, the membrane was exposed to enhanced chemiluminescent (ECL) substrates (Thermo Fisher Scientific) and developed by film.

Flow Cytometry Based STAT Phosphorylation Assay

At the NIH, PBMCs were thawed in XVIVO media (Lonza) with 10% human AB serum (Sigma), pelleted, washed with XVIVO, and resuspended in XVIVO media with 1% human AB serum at the concentration of 10^6 cells/mL. Then the cells were stimulated with 1000U IL-2 (Peprotech) for 10 minutes at 37°C, fixed with BD Fix/Lyse buffer (BD Bioscience) for 10 minutes at 37°C, and then washed with cold PBS with 0.2% BSA. Next, the fixed cells were permeabilized with -20°C methanol for 20 minutes on ice, washed 5 times with cold PBS with 0.2% BSA, and then stained with surface and intracellular flow cytometry antibodies for 30 minutes at 4°C The fixed, permeabilized, and stained cells were washed with PBS and resuspended in PBS with 0.2% BSA for flow cytometry analysis. In Newcastle, thawed PMBCs were rested for 4 hours in serum-free RPMI-media. After the addition of surface markers and a fixable viability dye, 2x 10^5 cells were stimulated for 10 minutes at 37°C with 100 ng/mL of

either IL-2, IL-7, IL-15 or left unstimulated. The Transcription Factor Phospho Buffer set (BD Biosciences) was used to fix and permeabilize cells according to the manufacturer's instructions. Cells were stained with the remaining surface as well as intracellular markers for 45 minutes at 4°C before cells were washed in TFP Perm/Wash buffer and finally resuspended in FACS buffer for acquisition.

Site-Directed Mutagenesis

The wild-type pME18S-IL2RB template plasmid (~5000 bp) was obtained from the NIH. Site-directed mutagenesis of T230C (p.L77P) was performed using the In-Fusion HD Cloning Kit (Takara Clontech) and following PCR primers (Sigma Aldrich):
F: AGCTGCCCCCCGTGAGTCAA and R: TCACGGGGGGCAGCTCACAGGTTT.
The linearized vector was generated by PCR using the CloneAmp HiFi PCR master mix (Takara ClonTech), plasmid template, and primers with the following thermocycling conditions: 35 cycles of 10 seconds at 98°C, 5 seconds at 55°C, and 25s at 72°C. The PCR products were separated on a 1% agarose gel by gel electrophoresis and the desired mutagenized product band was cut out. The PCR product was purified using the NucleoSpin Gel and PCR Clean Up (Takara) from the InFusion Cloning Kit. The linearized, mutagenized product was ligated using the InFusion Enzyme (Takara) to generate the L77P mutant pME18S-IL2RB plasmid. Stellar cells (Takara) were transformed with the new plasmid by heat shock; the transformed cells were plated on ampicillin plates and incubated overnight at 37°C. Plasmid was extracted from individual colonies using the QIAprep Spin MiniPrep Kit (Qiagen). The mutation was confirmed by Sanger sequencing.

Cloning

Using wild-type and mutant pME18S-IL2RB plasmids as the template, wtIL2RB and mutIL2RB PCR products with AsiSI and SpeI restriction sites were generated using the following primers: F: tagtaggcgatcgcgccaccATGGCGGCCCCTGCTCTGTC and R: ctactaactagtCACCAAGTGAGTTGGGTCCTGAC. The PCR products were purified by gel electrophoresis. Next the gel purified PCR products and pHTC-P2A plasmid (provided by John James) were digested with AsiSI and SpeI restriction enzymes in CutSmart Buffer (NEB) for 2 hours at 37°C and then purified by gel electrophoresis. IL2RB wt and mutant were ligated into separate custom-made pHTC/pBR322-P2A vectors using T4 DNA ligase (NEB). DH5alpha competent bacteria (NEB) were transformed with pHTC-wtIL2RB and pHTC-mutIL2RB and plated on Amp plates overnight. Individual colonies were Sanger sequenced to confirm successful cloning. pHTC-wtIL2RB, pHTC-mutIL2RB, and pGFP (provided by John James) were digested with mLuI and BamHI in NEB3.1 buffer and then purified by gel electrophoresis. Similar to above, GFP was ligated in to the pHTC vectors to generate pHTC-wtIL2RB-P2A-GFP and pHTC-mutIL2RB-P2A-GFP. The final plasmids were transformed in to DH5alpha bacteria, and individual colonies were Sanger sequenced again.

HEK293T Transfection and Confocal Imaging

HEK293T cells were cultured in complete DMEM or RPMI at 37°C in T75 flasks. $4x10^5$ cells in 2mL media were seeded into 6 well plates and grown overnight at 37°C At 40-50% confluence, the cells were transfected using 97uL OPTI-MEM (Gibco) and 3uL GeneJuice Transfection Reagent (VWR) per 1ug DNA. Cells were transfected with 1:pHTC-wtIL2RB-P2A-GFP and pHR-TetON-P2A-BFP, 2:pHTC-mutIL2RB-P2A-GFP and pHR-TetON-P2A-BFP, 3:pHTC-

wtIL2RB-P2A-GFP, 4:pHTC-mutIL2RB-P2A-GFP, and 5:pHR-TetON-P2A-BFP. Six hours after transfection with pHTC-IL2RB-P2A-GFP and pHR-TetON-P2A-BFP, cells were dosed with doxycycline (1ug/ml). The transfected cells were cultured overnight at 37°C, pelleted, washed with PBS, and stained with CD122-PE-Dazzle antibody for flow cytometry analysis. Similarly, HEK293T cells were transfected with pHR-wtIL2RB-GFP or pHR-mutIL2RB-GFP and pBFP-KDEL in the same conditions in fibronectin-coated dishes for confocal imaging. An Andor spinning disc confocal microscope system was used to image the live cells at 37°C. Under the same conditions, HEK293T cells were also transfected with pME-IL2RG, pME-JAK3, pME-STAT5-HA, pBFP, and different IL2RB plasmids to reconstitute the IL-2 receptor. After successful transfection, the cells were stimulated with high dose IL-2 and STAT phosphorylation was measured by flow cytometry as described above.

IL-2 binding assay
HEK293T cells were transfected with wild type and mutant IL-2RB and IL-2RG using the same transfection conditions as described above. $1x10^5$ transfected cells in 0.2 mL 0.2% BSA-PBS were incubated with 200, 100, 10, 1, or 0.01 nM biotinylated IL-2 (R&D Systems) for 30 minutes at 4°C. Then streptavidin-AlexaFluor 633 (1ug/mL, Invitrogen) was added and incubated for 15 minutes at 4 °C. Each sample was then washed 3x with 1mL PBS. The cells were resuspended in 300uL FACS buffer for subsequent FACS analysis. This protocol was adopted from Pillet et al. 2008.

NK degranulation and cytotoxicity assays
PBMCs were seeded at $1x10^5$ per well in a 96-well plate and primed with either IL-2 or IL-15 (100ng/ml each) for 12 hours or left unprimed. After the priming period, cells were co-incubated with K562 target cells (E:T ratio of 10:1) for 3 hours. Alongside with K562 exposure the CD107a-antibody was added to the wells. Cells were harvested and surface staining was carried out for 60 minutes on ice. Degranulation was measured by means of CD107a surface expression. Cytotoxicity was assessed by calculating the percentage of 7-AAD positive K562 after co-incubation minus the spontaneous K562 death rate when cultured alone. The addition of IL-2 or IL-15 was found to not affect the viability of K562 cells.

Interferon-γ production:
PBMCs ($1x10^5$ in 100 ul) were stimulated with either IL-2, IL-15 or IL-12 (100 ng/ml each, all from Peprotech) for six hours with Brefeldin A (BD GolgiStop) added for the final five hours. Cells were fixed and permeabilized using Cytofix/Cytoperm buffers (BD) according to the manufacturer's instructions and surface as well as intracellular staining were carried out for 30 minutes at 4°C.

Enzyme-linked immunosorbent assay (ELISA)
Serum was analyzed for IL-2 using IL-2 ELISA kit (Invitrogen) and for IL-15 using IL-15 High Performance Luminex kit (R&D Systems).

T cell proliferation
$2x10^5$ PBMC were incubated in triplicates per experimental condition with the indicated stimuli for 3 days before being pulsed with tritiated thymidine for 8 hours. A scintillation beta-counter was used to measure incorporation into dividing cells.

Molecular Modeling

Starting models were derived from a crystal structure of IL-2RB in complex with IL2-IL-2RB and IL-2 determined at 2.3 Å resolution (PDB: 5M5E) (Klein et al., 2017). For the S40L variant, the Leu40 side chain was modelled with COOT (Emsley and Cowtan, 2004) without molecular dynamics (MD) simulation. For the L77P variant, the Pro77 side chain was placed in the experimental electron density of Leu77 with COOT while minimizing clashes with surrounding atoms to achieve a favourable initial geometry. The GROMACS software package (Abraham et al., 2015) was used to set up and run MD simulations. The AMBER99SB-ILDN force field (Lindorff-Larsen et al., 2010) and TIP3P water model were used and the structures placed in dodecahedral boxes with 10 Å padding and surrounded with solvent including water and 150 mM NaCl. After steepest-gradient energy minimization, a modified Berendsen thermostat (2 groups, time constant 0.1 picoseconds, temperature 310 K) followed by a Berendsen barostat (isotropic, coupling constant 0.5 picoseconds, reference pressure 1 bar) were coupled to the system over 100 picoseconds. One hundred-nanosecond runs of unrestrained MD trajectories were produced. After removal of periodic boundary condition artefacts, MD runs were visualized and analysed in UCSF Chimera (Pettersen et al., 2004) and bulk statistics extracted using GROMACS analysis routines.

Lentiviral Transduction

Wild-type IL2RB was cloned into a pHR-GFP transfer plasmid. Lenti-X 293T cells (Clontech) were transfected with the pHR-IL2RB-GFP transfer plasmid, pSPAX2, and pMD2.g plasmid in OPTIMEM and PEI. Lentivirus was harvested at 24, 48, and 72 hours post-transfection. The viral supernatants were pooled and concentrated using Lenti-X concentrator (Clontech). An aliquot of the concentrated lentivirus was quantified by qPCR using the Lenti-X qRT-PCR Titration Kit (Clontech). PBMCs were thawed and cultured in complete RPMI with IL-7. The cells were activated with CD3/CD28 Dynabeads (Gibco) for at least 24 hours prior to lentiviral transduction. After activation, PBMCs were transduced with a ratio of 100:1 WT-IL2RB lentivirus:PBMCs on retronectin-coated plated by spinfection. The cells were transduced for 72 hours in complete RPMI with IL-7. Transduction efficiency was measured by FACS and transduced cells were subsequently assessed for STAT phosphorylation after IL-2 stimulation.

Online Supplemental Material

Figure S1 shows healthy control and patient T cell proliferative responses to PHA, anti-CD3, anti-CD3 and IL-2, and PMA and ionomycin. Figure S2 shows the molecular dynamic simulation results for wild-type, S40L, and L77P IL-2Rβ. Figure S3 shows the FACS plots for CD25 upregulation, CD107a degranulation and interferon-γ expression in healthy control and patient NK cells.

References

Abraham, M.J., Murtola, T., Schulz, R., Páll, S., Smith, J.C., Hess, B., and Lindahl, E. GROMACS: High performance molecular simulations through multi-level parallelism from laptops to supercomputers. *SoftwareX* 2015:1-2, 19-25.

Ahmadzadeh, M. & Rosenberg, S. A. IL-2 administration increases CD4(+)CD25(hi) Foxp3(+) regulatory T cells in cancer patients. *Blood* 2006; 107: 2409-14.

Bielekova, B. *et al.* Regulatory CD56bright natural killer cells mediate immunomodulatory effects of IL-2Rα-targeted therapy (daclizumab) in multiple sclerosis. *Proc Natl Acad Sci U S A*. 2006; 15: 5941-6.

Boyman, O, Kovar, M, Rubinstein, MP, et al. Selective stimulation of T cell subsets with antibody-cytokine immune complexes. *Science* 2006; 311: 1924-1927.

Boyman, O, Sprent, J. The role of interleukin-2 during homeostasis and activation of the immune system. *Nature Reviews* 2012; 12: 180-190.

Busse, D et al. Competing feedback loops shape IL-2 signaling between helper and regulatory T lymphocytes in cellular microenvironments. *Proc. Natl Acad. Sci.* 2010; 107: 3058-3063.

Caudy, A et al. CD25 deficiency causes an immune dysregulation, polyendocrinopathy, enteropathy, X-linked-like syndrome, and defective IL-10 expression from CD4 lymphocytes. *Journal of Allergy and Clinical Immunology*. 2007; 119: 482-487.

Dubois, S. *et al.* IL15 infusion of cancer patients expands the subpopulation of cytotoxic CD56bright NK cells and increases NK cell cytokine release capabilities. *Cancer Immunol. Res.* 2017; 10:929-38.

Emsley, P., and Cowtan, K. Coot: model-building tools for molecular graphics. *Acta Crystallogr D Biol Crystallogr* 2004: 60, 2126-2132.

Foley, B. *et al.* Cytomegalovirus reactivation after allogeneic transplantation promotes a lasting increase in educated NKG2C+natural killer cells with potent function. *Blood* 2012; **119:** 2665–2674.

Fontenot et al. A function for interleukin 2 in Foxp3- expressing regulatory T cells. *Nature Immunol.* 2005; 6: 1142-1151.

Gilmour KC et al. Defective expression of the interleukin-2/interleukin-15 receptor beta subunit leads to a natural killer-cell deficient form of severe combined immunodeficiency. *Blood* 2001; 98: 877-879.

Hatakeyema, M et al. Interleukin-2 receptor beta chain gene: generation of three receptor forms by cloned human alpha and beta chains cDNA. *Science* 1989; 1989: 551-556.

Hinks, A et al. Dense genotyping of immune-related disease regions identifies 14 new susceptibility loci for juvenile idiopathic arthritis. *Nature Genetics* 2013; 45(6): 664-669.

Ito, S. *et al.* Ultra-low dose interleukin-2 promotes immune-modulating function of regulatory t cells and natural killer cells in healthy volunteers. *Mol. Ther.* 2014; **22:** 1388–1395.

John, S et al. The Significance of Tetramerization in Promoter Recruitment by Stat5. *Mol. Cell Biol.* 1999; 19(3): 1910-1918.

Klein, C., Waldhauer, I., Nicolini, V.G., Freimoser-Grundschober, A., Nayak, T., Vugts, D.J., Dunn, C., Bolijn, M., Benz, J., Stihle, M., et al. Cergutuzumab amunaleukin (CEA-IL2v), a CEA-targeted IL-2 variant-based immunocytokine for combination cancer immunotherapy: Overcoming limitations of aldesleukin and conventional IL-2-based immunocytokines. *Oncoimmunology* 2017: 6, e1277306.

Lee, J et al. Epigenetic modification and antibody-dependent expansion of memory-like NK cells in human cytomegalovirus-infected individuals. *Immunity* 2015; 42: 431-442.

Levin, AM et al. Exploiting a natural conformational switch to engineer an interleukin-2 'superkine.' *Nature* 2012; 24: 352-359.

Liao, W et al. Interleukin-2 at the Crossroads of Effector Responses, Tolerance, and Immunotherapy. *Immunity*. 2013; 38: 13-25.

Lindorff-Larsen, K., Piana, S., Palmo, K., Maragakis, P., Klepeis, J.L., Dror, R.O., and Shaw, D.E. Improved side-chain torsion potentials for the Amber ff99SB protein force field. *Proteins* 2010; 78, 1950-1958.

Lopez-Vergès, S. *et al.* CD57 defines a functionally distinct population of mature NK cells in the human CD56dimCD16+NK-cell subset. *Blood* 2010; **116:** 3865–3874.

Louie, RJ et al. Novel Pathogenic Variants in FOXP3 in Fetuses with Echogenic Bowel and Skin Desquamation Identified by Ultrasound. *Am J Med Genet A.* 2017; 173(5): 1219-1225.

Majri, S et al. STAT5B: A Differential Regulator of the Life and Death of CD4 + Effector Memory T Cells. *J Immunol.* 2017; 200(1):110-118.

Malek et al. CD4 Regulatory T Cells Prevent Lethal Autoimmunity in IL-2R -Deficient Mice: Implications for the Nonredundant Function of IL-2. *Immunity* 2002; 17:167-178.

Moffatt, MF et al. A large-scale, consortium-based genomewide association study of asthma. *NEJM* 2010; 363(13): 1211-1221.

Pettersen, E.F., Goddard, T.D., Huang, C.C., Couch, G.S., Greenblatt, D.M., Meng, E.C., and Ferrin, T.E. UCSF Chimera--a visualization system for exploratory research and analysis. *J Comput Chem* 2004; 25: 1605-1612.

Pillet, AH et al. Human IL-Rb chains form IL-2 binding homodimers. *Eur. Cytokine Netw.* 2008; 19: 49-59.

Renoux, VM et al. Identification of a Human Natural Killer Cell Lineage-Restricted Progenitor in Fetal and Adult Tissues. *Immunity* 2015; 43: 394-407.

Scharfe, N et al. Human immune disorder arising from mutation of the alpha chain of the interleukin-2 receptor. *Proc. Natl Acad. Sci.* 1997; 94: 3168-3171.

Schlums, H et al. Cytomegalovirus infection drives adaptive epigenetic diversification of NK cells with altered signaling and effector function. *Immunity* 2015; 42: 443-456.

Sockolosky, JT et al. Selective targeting of engineered T cells using orthogonal IL-2 cytokine receptor complexes. *Science* 2018; 359:1037-1042.

Suzuki, H et al. Deregulated T cell activation and autoimmunity in mice lacking interleukin-2 receptor beta. *Science* 1995; 268: 1472-1476.

Suzuki, H et al. Abnormal Development of Intestinal Intraepithelial Lymphocytes and Peripheral Natural Killer Cells in Mice Lacking the IL-2 Receptor Beta Chain. *JEM* 1997; 185: 499-505.

Takeshita, T et al. Cloning of the gamma chain of the human IL-2 receptor. *Science* 1992; 257:379-382.

Vazquesz-Lombardi, R et al. Potent antitumor activity ofinterleukin-2-Fc fusion proteins requires Fc-mediated depletion of regulatory T cells. *Nat. Commun* 2017; 8:15373.

Waldmann, TA. The biology of interleukin-2 and interleukin-15. *Nature Rev. Immunol.* 2006; 6: 595-601.

Wang, X, Rickert, M, Garcia, KC. Structure of the quaternary complex of interleukin-2 with its a, b, and g receptors. *Science* 2005; 310:1159-1163.

Willerford, DM et al. Interleukin-2 receptor alpha chain regulates the size and content of the peripheral lymphoid compartment. *Immunity* 1995; 3:521-530.

Ye, C, Brand, D, Zhong, S. Targeting IL-2: an unexpected effect in treating immunological diseases. *Signal Transduction and Targeted Therapy* 2018; Online: https://www.nature.com/articles/s41392-017-0002-5#ref-CR77

Figure Legends

Figure 1. Genetic and clinical features of the disease cohort.
A. Four consanguineous pedigrees of eight affected individuals (A1-D3) with three different homozygous recessive mutations. B. Radiographic evidence for pulmonary disease in Kindred A. Panels 1 and 2 show a left pleural effusion. Hepatosplenomegaly can also be seen in Panel 1. Panels 3 and 4 show numerous small pulmonary nodules and tree-in-bud changes suggestive of pneumonia. Red arrows highlight 2 small lung nodules. Panel 5 shows enlarged axillary lymph nodes (red arrows). C. Immunohistochemistry of fetal skin from kindred D, patients D1, D2, and D3 stained in brown for the lymphocyte markers as indicated. **Black scale bar = 50um.**
D. Immunohistochemistry of duodenal (left) and rectal (right) biopsies of patient B1 and healthy control, stained with indicated markers. Purple: CD20, CD4, and FoxP3; Yellow: CD3, CD8, and CD4 for the respective panels. **Black scale bar = 100um.** E. Summary of clinical hallmarks of IL-2R□ deficiency in the five pediatric patients. Skin abnormalities were observed in the individuals in kindred D in addition to the pediatric patients (8 total).

Figure 2. IL-2Rβ coding mutations cause IL-2Rβ surface receptor deficiency.
A. Schematic of intracellular (ICD) and extracellular domains (ECD) of the IL-2Rβ protein depicting the location of the three mutations in the ECD. The signal peptide is highlighted in orange and the canonical WSXWS motif is highlighted in green. B. Crystal structure of IL-2:IL-2R complex with the expanded view showing the position of the three mutations in white: L77P, S40L, and Q96*; (modified from PDB 2B5I, Wang et al. 2005). Red: IL-2/15Rβ, blue: IL-2Rγ, green: IL-2Rα, and yellow: IL-2 with IL-2Rβ interface colored in red. C. Histogram of IL-2Rβ surface expression in $CD3^+$ $CD4^+$ (red) ,$CD3^+$ $CD8^+$ (blue), and $CD3^-$ $CD56^+$ NK cells (green) from patient B1 compared to healthy control (top 3 panels: healthy control, bottom 3 panels). D. Histogram of IL-2Rβ surface expression in NK cells ($CD3^-$ $CD56^+$) (red = homozygous affected A1, blue = heterozygote healthy A0, black=healthy control). Data representative of 4 independent experiments. E. Western blot of FACS-sorted $CD3^-$ $CD56^+$ NK cells from A1, heterozygote parent (A0), B1, and four healthy controls (HC1-4). F. Western blot of FACS-sorted $CD3^+$ $CD8^+$ T cells from A1, heterozygote parent (A0), and three healthy controls (HC1-3). G. Western blot of FACS-sorted $CD3^+$ $CD4^+$ T cells from A1, heterozygote parent (A0), B1, and three healthy controls (HC1-3). H. Western blot of fetal thymuses from Kindred D (D1-D3) and five fetal thymic controls from 25 weeks old (FT3-FT4) and 31 weeks old (FT1, FT2, FT5). E-H, loading control: Actin. Western blots (2E-2H) were repeated in triplicate.

Figure 3. Investigation of IL-2Rβ deficiency mechanisms in a HEK293T transfection model.
A. FACS plot of GFP and IL-2Rβ expression by HEK293T cells transfected with pHTC-wtIL2RB (red) and pHR-TetON-BFP or transfected with pHTC-mutIL2RB (blue) and pHR-TetON-BFP. B. Histograms of BFP, GFP, or IL-2RB expression given the listed four transfection conditions: wild-type, mutant, TetON only, and no transfection. C. Western blot of HEK293T cells transfected with pHTC-wtIL2RB-GFP or pHTC-mutIL2RB-GFP. Loading controls: actin and GFP. D. Confocal images of live HEK293T cells co-transfected with KDEL-BFP (ER localization marker) and WT-IL2RB-GFP or Mut-IL2RB-GFP. **White scale bar = 10um.** E. Graph of normalized surface IL-2RB expression in HEK293T cells with exogenous IL-2 receptor system for the three disease-causing IL-2RB mutations. *$p<0.05$, Mann-Whitney U

test. F. Graph of pSTAT5 response to high dose IL-2 in HEK293T cells with exogenous IL-2 receptor system. *p<0.05, Mann-Whitney U test. G. Molecular dynamic simulation of the receptor cytokine binding interface in WT IL-2Rβ and the S40L variant. The IL-2R subunit is coloured in blue, IL-2Rβ in red and IL-2 in yellow (PDB: 5M5E). The structure of S40L mutant after 100 ns of molecular dynamics (MD) simulation (green) is shown superimposed on the structure of the WT IL-2Rβ after 100 ns MD simulation (red). The leucine side chain clashes with main chain atoms in the BC2 loop (residues 157-165) of the D2 domain, which contributes directly to IL-2 binding. A zoomed in panel of the IL-2 and MD simulated S40L mutant IL-2Rβ interface is provided. H. Graph of IL-2 binding by WT IL-2Rβ, S40L mutant, and no IL-2Rβ negative control in HEK293T cells measured by flow cytometry using a biotin-streptavidin system. Experiments (3A-3F and 3H) were repeated in triplicate with graphs showing mean ± SEM.

Figure 4. IL-2Rβ deficiency abrogates IL-2 induced STAT3 and STAT5 phosphorylation in peripheral T cells.
Flow cytometry-based measure of STAT3 phosphorylation in $CD3^+$ $CD4^+$ T cells from healthy controls (HC), heterozygote parent A0 (WT/Mut), and homozygous affected A1 (Mut/Mut). B. STAT5 phosphorylation in $CD3^+$ $CD4^+$ T cells. C. STAT3 phosphorylation in CD8 T cells. D. STAT5 phosphorylation in $CD8^+$ T cells. (red=representative healthy control, blue=representative affected, lighter shade=unstimulated, darker shade=stimulated with 1000U IL-2). E. STAT5 phosphorylation in $CD4^+$ and $CD8^+$ T cells (B1) in response to IL-2, IL-7, and IL-15 stimulation. F. Flow cytometry plot of CD25 and FoxP3 expression in healthy control and homozygous affected (B1). Data representative of 3 independent experiments. G. Graphs of IL-2 and IL-15 levels in healthy controls, A0 (healthy heterozygous father of A1), patient A1, and patient B1 serum. H. Graphs of percent of $CD25^{high}$ cells in healthy control (blue), patient B1 (red square), and patient A1 (red triangle) $CD4^+$ T cells, $CD8^+$ T cells, and NK cells that have been primed with IL-2 or IL-15 for 12 hours or left unprimed. ****$p < 0.0001$, ***$p < 0.001$, **$p < 0.01$, *$p < 0.05$, Mann-Whitney U tests were performed in A-D, and G. Student t-test was performed in H. Experiments (4A-4H) were performed in triplicate with graphs showing mean ± SD.

Figure 5. NK cells retain IL-2/IL-15 responsiveness and effector function but is deficient in adaptive "memory-like" NK subsets.
A. Flow cytometry plot of CD16 and CD56 expression in $CD3^-$ $CD19^-$ lymphocytes (patient B1), representative of 4 independent experiments B. Histograms of Granzyme B and Perforin content in CD56bright versus CD56dim NK cells. Healthy control in blue, patient B1 in red. Experiment displayed representative of 3 independent experiments. C. STAT5 phosphorylation in NK cells (B1) in response to IL-2, IL-7, and IL-15 stimulation. D. CD107a expression (degranulation) in healthy control and patient B1 NK cells co-cultured with K562 cells after 12 hours of priming with IL-2 or IL-15 or left unprimed. E. Percentage of 7-AAD-positive, i.e. dead, K562 cells as a measure of cytotoxicity when co-cultured with healthy control (blue circles) NK cells or patient B1 (red squares) NK cells. F. Interferon-γ production in response to the indicated stimuli in control NK cells (blue circles) or patient B1 NK cells (red squares). G. Expression of NKG2C and CD57 on NK cells of CMV+ control and patient B1. H. Summary graph displaying the percentage of $CD57^+$ positivity within the $NKG2C^+$ and NKG2C- NK cell subsets (mean ± SD). Data representative of 6 independent experiments. I. FACS plots of FcεRIγ, PLZF and Syk

expression in CMV- and CMV+ healthy controls and well as patient B1, gated on NKG2C-expressing NK cells. J. Summary graphs showing the percentage of NKG2C$^+$ NK cells downregulating the indicated proteins. ****$p < 0.0001$, ***$p < 0.001$, **$p < 0.01$, *$p < 0.05$, student t-tests were performed. Experiments 5D-5F were performed in duplicate and 5A-5C, 5G-5J were performed in triplicate with graphs showing mean ± SD.

Figure 6. Lentiviral rescue of IL-2Rβ and STAT phosphorylation in primary T cells. A. Histogram showing GFP expression in patient A1 CD3$^+$ T cells transduced (red) with lentiviral wild-type IL-2Rβ and GFP and no transduction control (blue). B. Histogram showing IL-2Rβ expression in patient A1 CD3$^+$ T cells transduced (red) with lentiviral wild-type IL-2RB and GFP and no transduction control (blue). C. Histograms showing STAT3 phosphorylation in response to IL-2 stimulation in transduced (dark red) and non-transduced (dark blue) CD3$^+$ A1 T cells. D. Histograms showing STAT5 phosphorylation in response to IL-2 stimulation in transduced (dark red) and non-transduced (dark blue) CD3$^+$ A1 T cells. E. Graph of delta MFI of pSTAT5 between IL-2 stimulated and unstimulated in healthy controls and L77P patients A1 and B1 transduced and no transduction control. *$p<0.05$, Mann-Whitney U test, n.s.= not significant. Experiments 6A-6E were performed in triplicate with the graph showing mean ± SEM.

Supplementary Figure S1. T cell proliferative responses. Graph of T cell proliferative responses to PHA, anti-CD3, anti-CD3 and IL-2, and PMA/ionomycin in patient B1 and healthy control cells based on thymidine incorporation.

Supplementary Figure S2. Molecular dynamic simulation of WT, S40L, and L77P IL-2Rβ structures. A. Root mean square deviation (RMSD) between the WT, S40L, and L77P IL-2Rβ structures over 100 nanoseconds of unrestrained MD simulation with explicit solvent. B. Root mean square fluctuation (RMSF) in WT, S40L, and L77P IL-2Rβ over the complete trajectory.

Supplementary Figure S3. A. FACS plots demonstrating upregulation of CD25 in CD3-CD56+ NK cells from a healthy control (top panel) or patient B1 (bottom panel) either unprimed or after priming with IL-2 or IL-15 (100 ng/ml each) for 12 hours followed by a 3 hour co-incubation period with K562 cells. B. FACS plots showing surface expression of CD107a in CD3-CD56+ NK cells from a healthy control (top panel) or patient B1 (bottom panel) either unprimed or after priming with IL-2 or IL-15 (100 ng/ml each) for 12 hours in response to co-incubation period K562 cells for 3 hours. C. Intracellular staining for Interferon-γ in CD3-CD56+ NK cells from a healthy control (top panel) or patient B1 (bottom panel) after stimulation with IL-2, IL-15 or IL-12 (100 ng/ml each) for 6 hours.

Figure 1

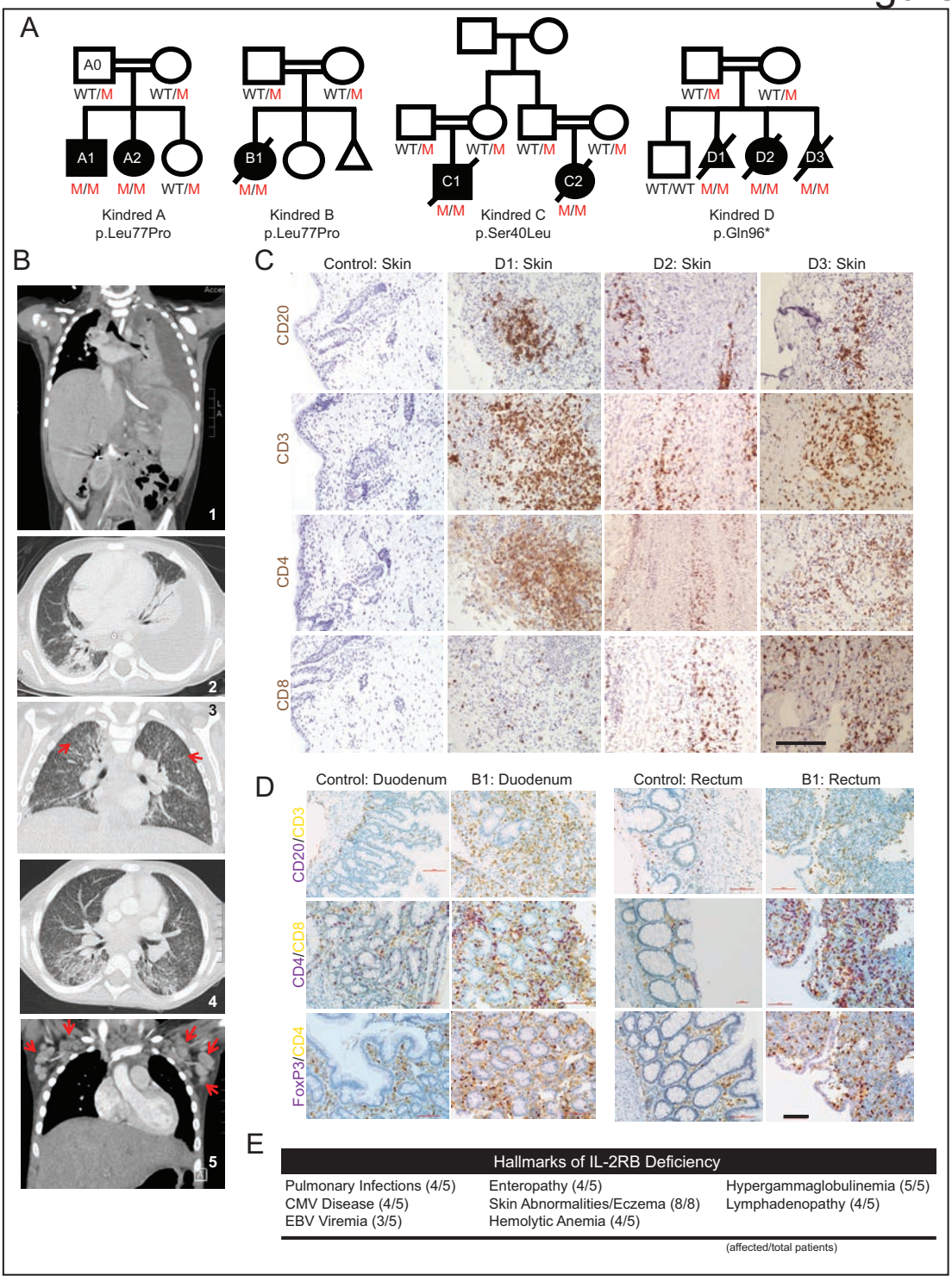
A
A0
WT/M
WT/M
A1
A2
M/M
M/M
WT/M
Kindred A
p.Leu77Pro
B1
M/M
Kindred B
p.Leu77Pro
C1
C2
M/M
M/M
Kindred C
p.Ser40Leu
D1
D2
D3
WT/WT
M/M
M/M
M/M
Kindred D
p.Gln96*
B
1
2
3
4
5
C
Control: Skin
D1: Skin
D2: Skin
D3: Skin
CD20
CD3
CD4
CD8
D
Control: Duodenum
B1: Duodenum
Control: Rectum
B1: Rectum
CD20/CD3
CD4/CD8
FoxP3/CD4
E
Hallmarks of IL-2RB Deficiency
Pulmonary Infections (4/5)
CMV Disease (4/5)
EBV Viremia (3/5)
Enteropathy (4/5)
Skin Abnormalities/Eczema (8/8)
Hemolytic Anemia (4/5)
Hypergammaglobulinemia (5/5)
Lymphadenopathy (4/5)
(affected/total patients)

Figure 2

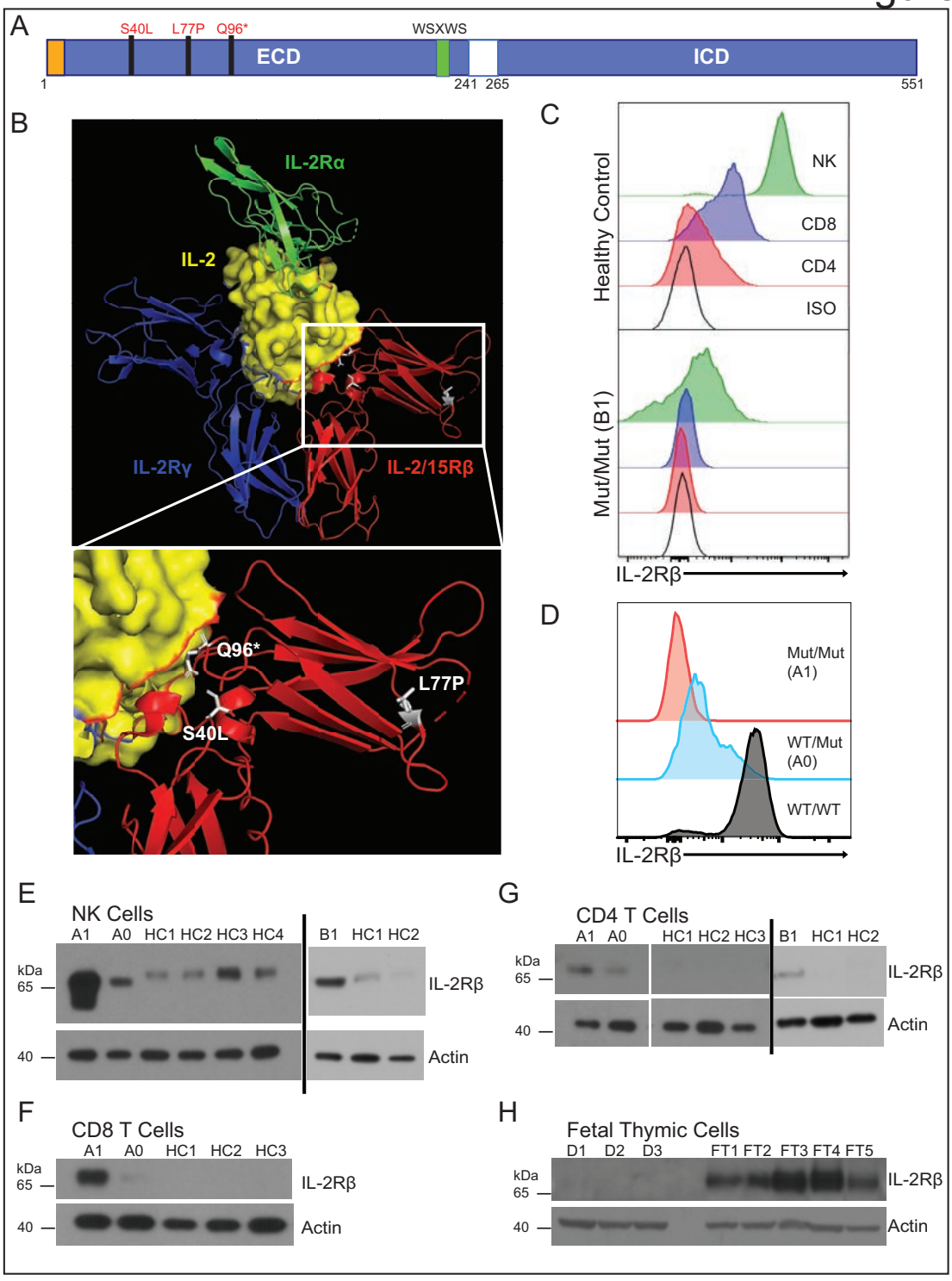
A
S40L
L77P
Q96*
WSXWS
ECD
ICD
1
241
265
551
B
IL-2Rα
IL-2
IL-2Rγ
IL-2/15Rβ
Q96*
L77P
S40L
C
Healthy Control
NK
CD8
CD4
ISO
Mut/Mut (B1)
IL-2Rβ
D
Mut/Mut (A1)
WT/Mut (A0)
WT/WT
IL-2Rβ
E
NK Cells
A1 A0 HC1 HC2 HC3 HC4
B1 HC1 HC2
kDa
65
40
IL-2Rβ
Actin
F
CD8 T Cells
A1 A0 HC1 HC2 HC3
kDa
65
40
IL-2Rβ
Actin
G
CD4 T Cells
A1 A0 HC1 HC2 HC3
B1 HC1 HC2
kDa
65
40
IL-2Rβ
Actin
H
Fetal Thymic Cells
D1 D2 D3
FT1 FT2 FT3 FT4 FT5
kDa
65
40
IL-2Rβ
Actin

Figure 3

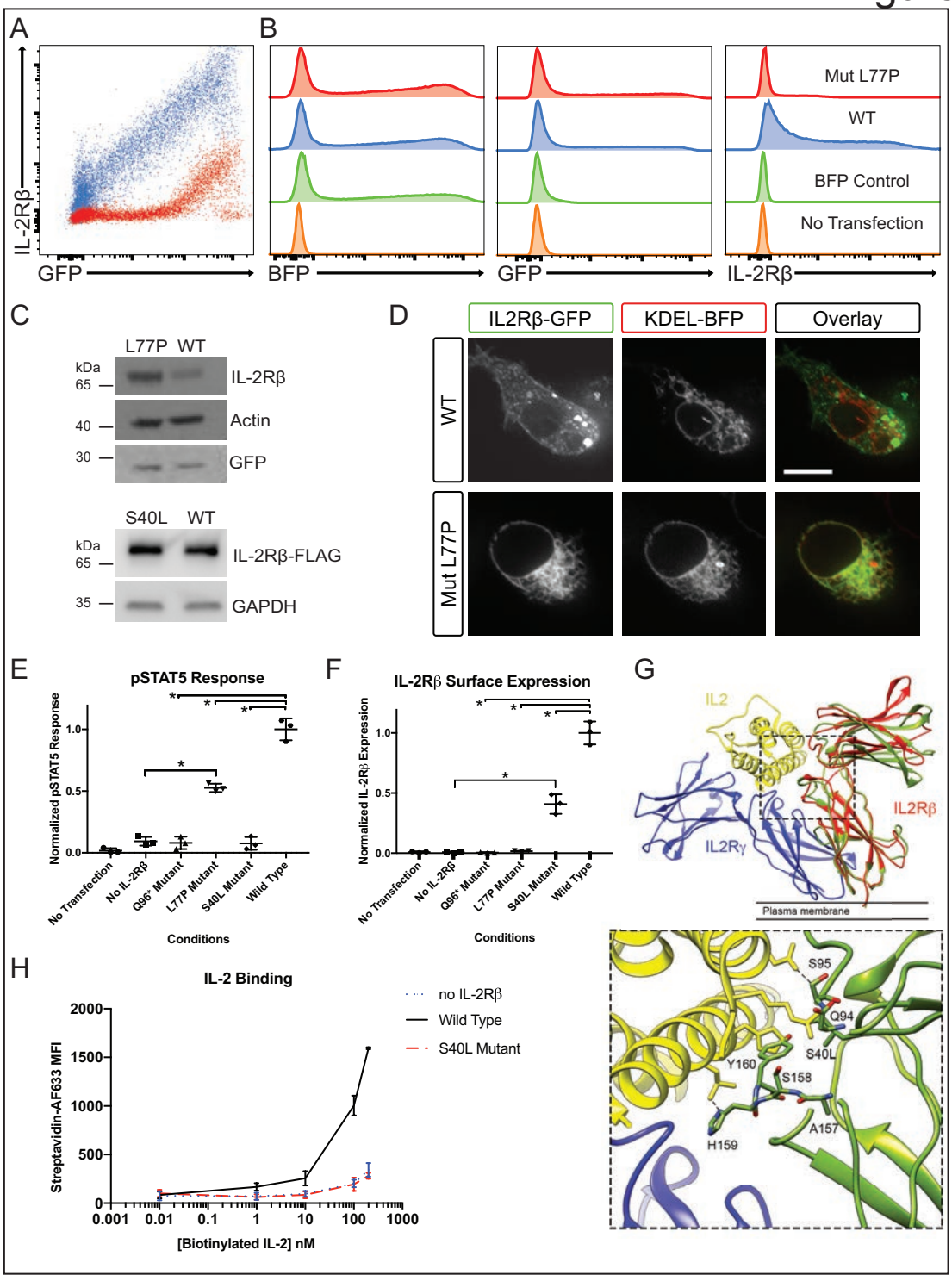
A
B
IL-2Rβ
GFP
BFP
GFP
IL-2Rβ
Mut L77P
WT
BFP Control
No Transfection
C
L77P WT
kDa
65
IL-2Rβ
40
Actin
30
GFP
S40L WT
kDa
65
IL-2Rβ-FLAG
35
GAPDH
D
IL2Rβ-GFP
KDEL-BFP
Overlay
WT
Mut L77P
E
pSTAT5 Response
Normalized pSTAT5 Response
1.0
0.5
0.0
No Transfection
No IL-2Rβ
Q96* Mutant
L77P Mutant
S40L Mutant
Wild Type
Conditions
F
IL-2Rβ Surface Expression
Normalized IL-2Rβ Expression
1.0
0.5
0.0
No Transfection
No IL-2Rβ
Q96* Mutant
L77P Mutant
S40L Mutant
Wild Type
Conditions
G
IL2
IL2Rβ
IL2Rγ
Plasma membrane
S95
Q94
S40L
Y160
S158
A157
H159
H
IL-2 Binding
Streptavidin-AF633 MFI
2000
1500
1000
500
0
0.001
0.01
0.1
1
10
100
1000
[Biotinylated IL-2] nM
no IL-2Rβ
Wild Type
S40L Mutant

!

Figure 4

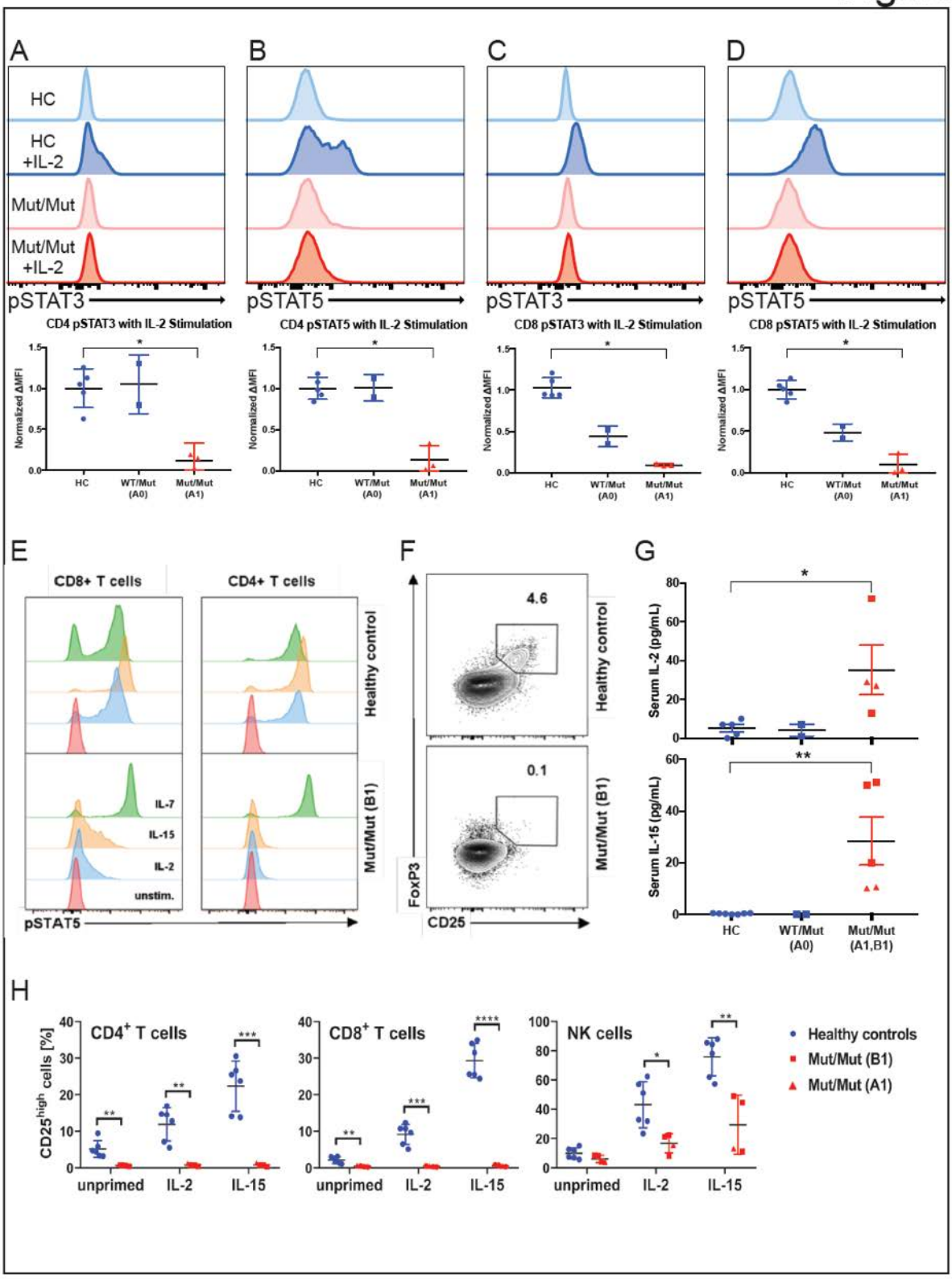
A
B
C
D
HC
HC +IL-2
Mut/Mut
Mut/Mut +IL-2
pSTAT3
pSTAT5
pSTAT3
pSTAT5
CD4 pSTAT3 with IL-2 Stimulation
CD4 pSTAT5 with IL-2 Stimulation
CD8 pSTAT3 with IL-2 Stimulation
CD8 pSTAT5 with IL-2 Stimulation
Normalized ΔMFI
HC
WT/Mut (A0)
Mut/Mut (A1)
E
CD8+ T cells
CD4+ T cells
Healthy control
Mut/Mut (B1)
IL-7
IL-15
IL-2
unstim.
pSTAT5
F
4.6
0.1
Healthy control
Mut/Mut (B1)
FoxP3
CD25
G
Serum IL-2 (pg/mL)
Serum IL-15 (pg/mL)
HC
WT/Mut (A0)
Mut/Mut (A1,B1)
H
CD4+ T cells
CD8+ T cells
NK cells
CD25high cells [%]
unprimed
IL-2
IL-15
Healthy controls
Mut/Mut (B1)
Mut/Mut (A1)

Figure 5

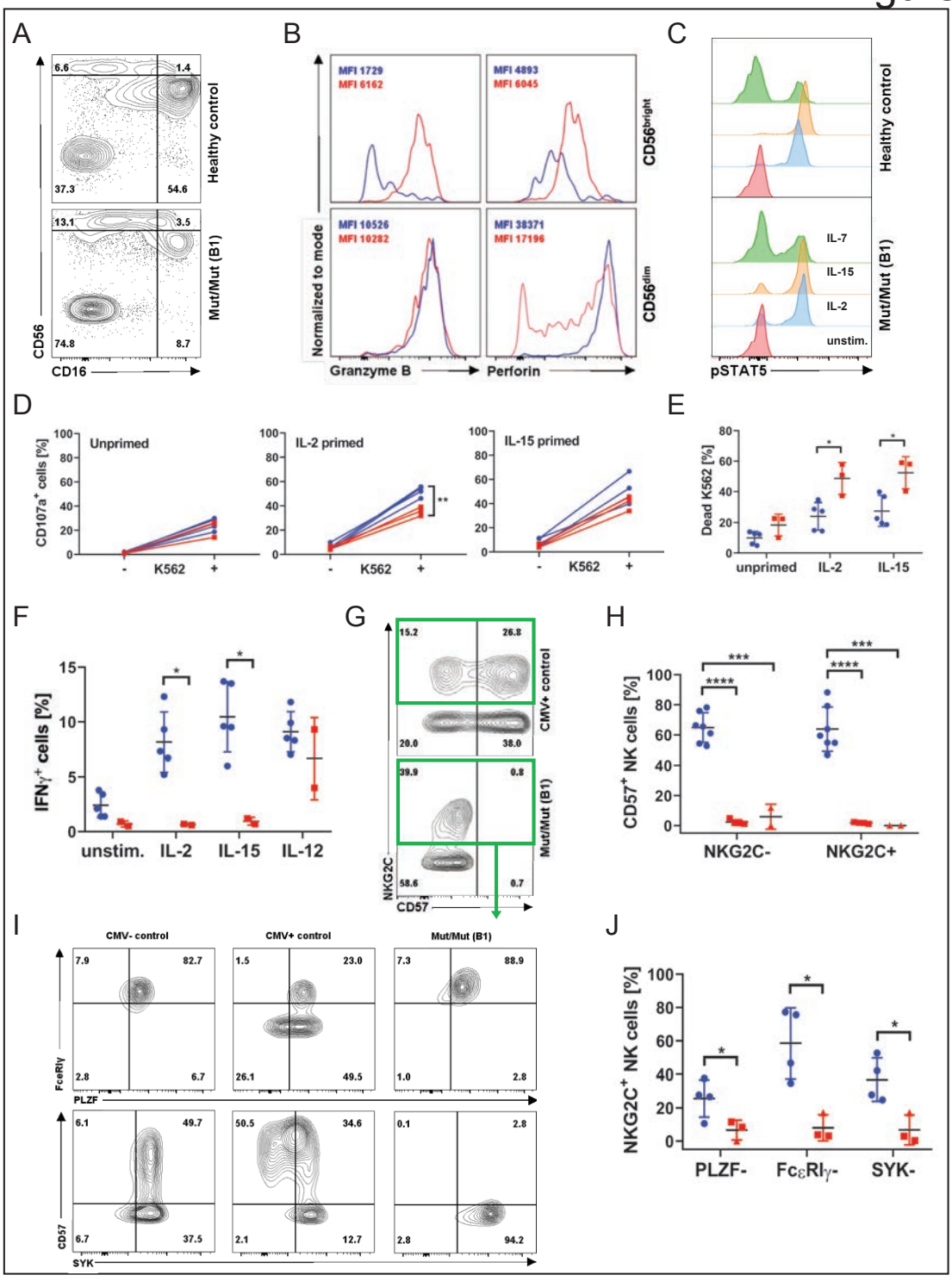
A
6.6
1.4
37.3
54.6
Healthy control
13.1
3.5
74.8
8.7
Mut/Mut (B1)
CD56
CD16
B
MFI 1729
MFI 6162
MFI 4893
MFI 6045
CD56bright
MFI 10526
MFI 10282
MFI 38371
MFI 17196
CD56dim
Normalized to mode
Granzyme B
Perforin
C
Healthy control
IL-7
IL-15
IL-2
unstim.
Mut/Mut (B1)
pSTAT5
D
Unprimed
IL-2 primed
IL-15 primed
CD107a+ cells [%]
K562
E
Dead K562 [%]
unprimed
IL-2
IL-15
F
IFNγ+ cells [%]
unstim.
IL-2
IL-15
IL-12
G
15.2
26.8
CMV+ control
20.0
38.0
39.9
0.8
Mut/Mut (B1)
58.6
0.7
NKG2C
CD57
H
CD57+ NK cells [%]
NKG2C-
NKG2C+
I
CMV- control
CMV+ control
Mut/Mut (B1)
7.9
82.7
2.8
6.7
1.5
23.0
26.1
49.5
7.3
88.9
1.0
2.8
FcεRIγ
PLZF
6.1
49.7
6.7
37.5
50.5
34.6
2.1
12.7
0.1
2.8
2.8
94.2
CD57
SYK
J
NKG2C+ NK cells [%]
PLZF-
FcεRIγ-
SYK-

Figure 6

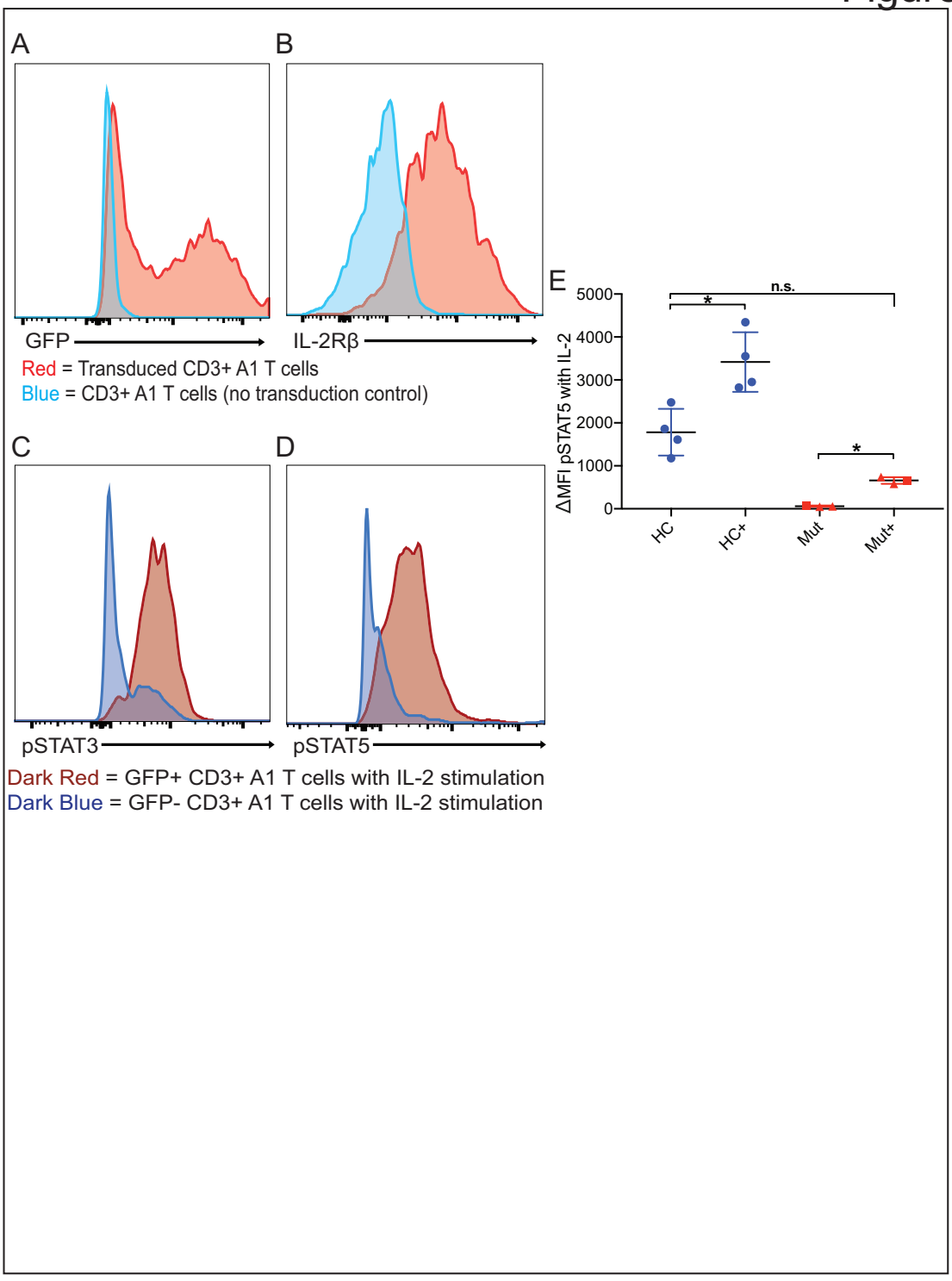
A
B
GFP
IL-2Rβ
Red = Transduced CD3+ A1 T cells
Blue = CD3+ A1 T cells (no transduction control)
C
D
pSTAT3
pSTAT5
Dark Red = GFP+ CD3+ A1 T cells with IL-2 stimulation
Dark Blue = GFP- CD3+ A1 T cells with IL-2 stimulation
E
ΔMFI pSTAT5 with IL-2
5000
4000
3000
2000
1000
0
n.s.
*
*
HC
HC+
Mut
Mut+

Supplementary Figure 1.

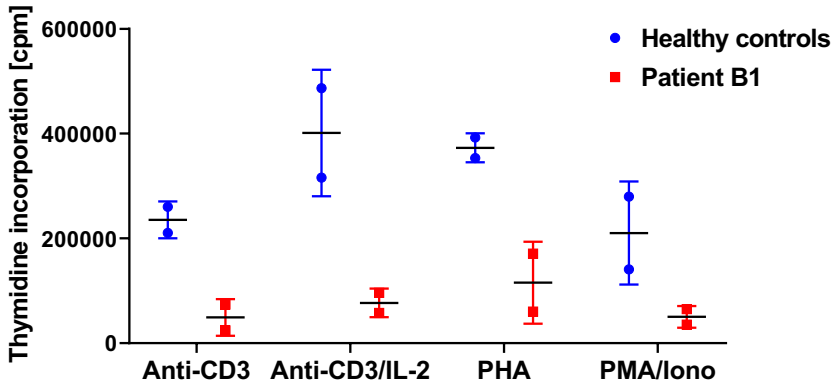

Supplementary Figure 2.

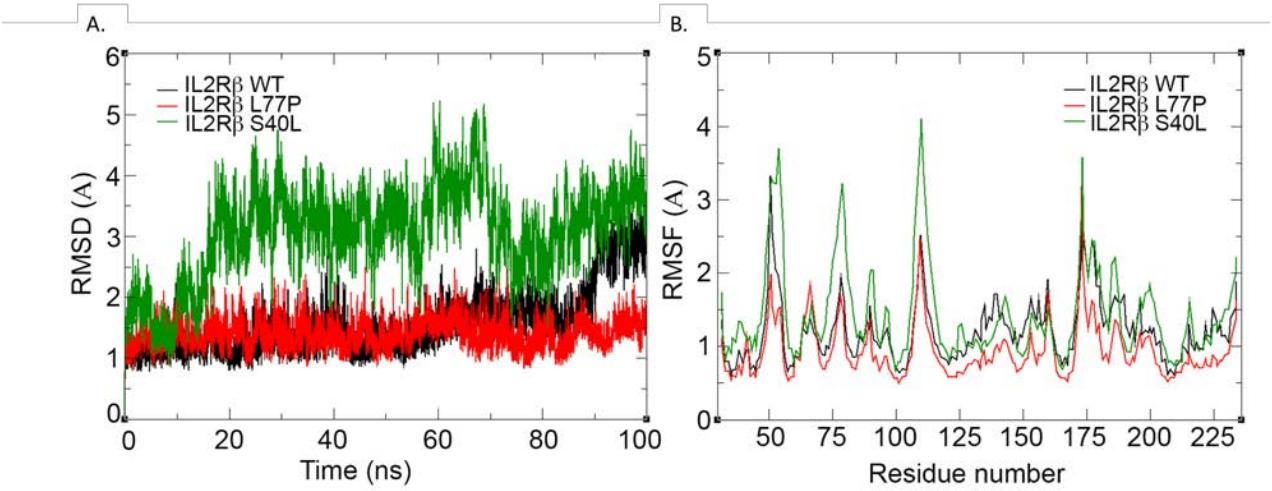

Supplementary Figure 3.

A.

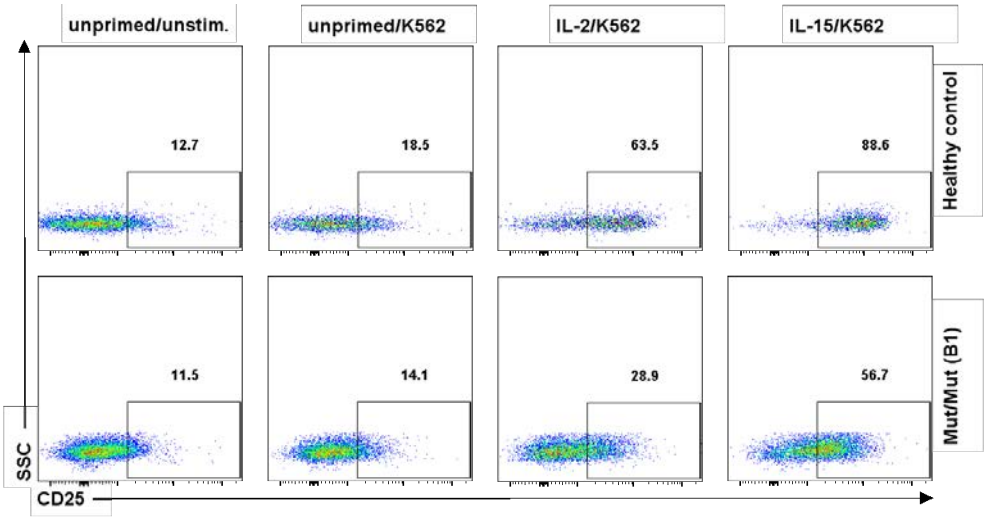

B.

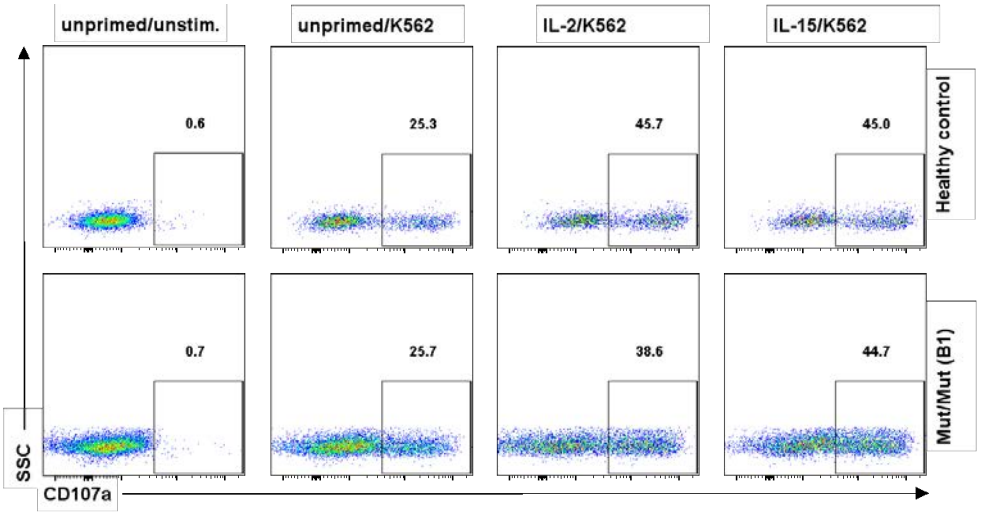

C.

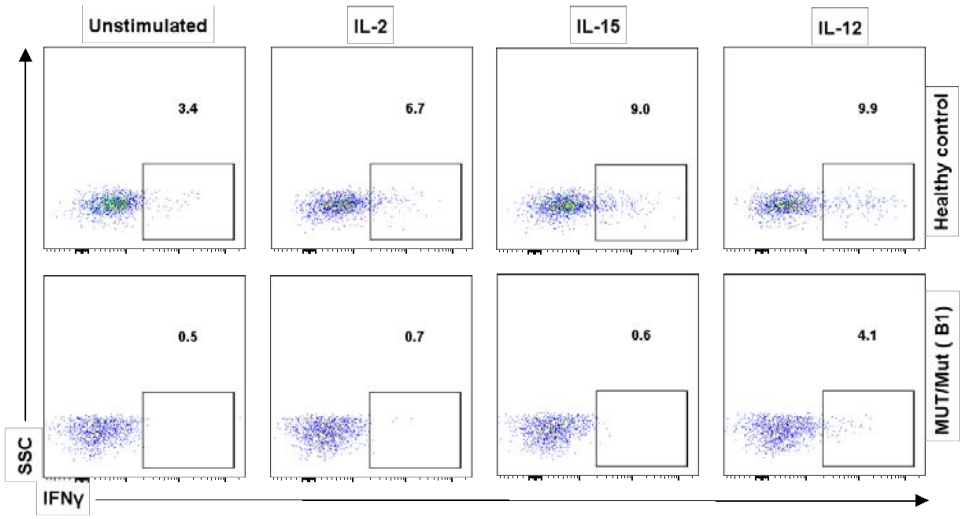

Supplementary Tables

Table 1. Patient mutations and clinical manifestations

Kindred	Patient	Mutation	Origin	Onset	Infectious Disease	Autoimmunity	Other Manifestations	Lab Values	Outcome
A	A1	p.L77P	Pakistani	32 months old	Severe gastroenteritis with norovirus, adenovirus, and EBV viremia	Thyrotoxicosis secondary to Graves' disease (+anti-thyroglobulin, +anti-TPO), and borderline ANCA status	Severe dermatitis, hepatosplenomegaly, lymphadenopathy, and asthma	Anemia, eosinophilia, hyper-IgG, hyper-IgA, and hyper-IgE	Alive
	A2	p.L77P	Pakistani	6 months old	Recurrent pulmonary infections, panuveitis, proctocolitis, mucocutaneous candidiasis, ESBL UTI, and CMV and EBV viremia	ANCA+ vasculitis (+MPO-ANCA), Celiac disease (+anti-TTG IgA), and +anti-smooth muscle Ab.	Dermatitis, hepatosplenomegaly and lymphadenopathy	Hyper-IgG, hyper-IgA, and hyper-IgE	Alive post-HSCT
B	B1	p.L77P	Bengali	1 month old	Pulmonary infection, ESBL and candida UTI, and CMV hepatitis and viremia	Autoimmune hemolytic anemia, ANA+, +anti-smooth muscle Ab, and autoimmune enteropathy	Severe dermatitis and hepatosplenomegaly	Hyper-IgG, hyper-IgA, and hyper-IgM	Deceased post-HSCT from pneumonitis and respiratory failure
C	C1	p.S40L	Saudi	6 months old	Recurrent pulmonary and ear infections, and CMV and EBV viremia	Autoimmune hemolytic anemia and food allergy	Severe dermatitis, hepatosplenomegaly, and lymphadenopathy	Hyper-IgG, hyper-IgA, and hyper-IgE	Deceased at 3 years old from pneumonitis and sepsis
	C2	p.S40L	Saudi	2 months old	Recurrent pulmonary and ear infections, enteropathy, and CMV viremia	Autoimmune hemolytic anemia and food allergy	Severe dermatitis, hepatosplenomegaly, and lymphadenopathy	Hyper-IgG, hyper-IgA, and hyper-IgE	Deceased at 18 months old from pneumonitis and respiratory failure
D	D1	p.Q96X	Romani	fetal	N/A	Lymphocytic infiltration in the skin and various organs	Hepatosplenomegaly, meningio-myelocele, Hydrocephalus, Chiari malformation, and ichthyosis	N/A	Terminated at 25 weeks
	D2	p.Q96X	Romani	fetal	N/A	Lymphocytic infiltration in the skin and various organs	Hepatosplenomegaly, severe arthrogyposis, diaphragmatic immobility, and ichthyosis	N/A	Died two hours after pre-mature birth at 31 weeks from respiratory failure
	D3	p.Q96X	Romani	fetal	N/A	Lymphocytic infiltration in the skin and various organs	Hepatosplenomegaly and ichthyosis	N/A	Terminated at 30 weeks

CMV = cytomegalovirus, EBV = Epstein Bar Virus, TPO = thyroperoxidase, Ab= antibody, ANCA = anti-neutrophil cytoplasmic antibody, MPO=myeloperoxidase, ANA= anti=nuclear antibody, TTG= tissue transglutaminase, ESBL= extended spectrum beta lactamase bacteria, UTI= urinary tract infection, HSCT= hematopoietic stem cell transplant. N/A = Not available.

Table 2. Lab values and absolute cell counts

Lab Values	A1	A2	B1	C1	C2	Reference
CMV*	Negative	37407	Positive	10000	2340	Negative (0 copies/ml)
EBV	2664	80254	Negative	157180	Negative	Negative (0 copies/ml)
IgM	0.34	1.0	6.6	0.7	0.86	(0.37-1.84 g/L)
IgA	4	8.4	1.55	4.96	3.86	(0.2-1.2 g/L)
IgG	22.3	23	26.9	22.2	12.3	(2.5-9.1 g/L)
IgE	12180	3031	20	24990	8370	(1.6-30 kU/L)
Anemia	Coombs+	Negative	Coombs +	Coombs +	Coombs +	Negative
Absolute Cell Counts						
CD3+	1272	3897	3454	1583	4098	1700-1900 cells/ul
CD3+/CD4+	954	2328	1436	950	2466	800-1700 cells/ul
CD3+/CD8+	291	1429	1906	361	1128	700-1000 cells/ul
CD19+	859	1274	533	728	1760	400-800 cells/ul
CD16+/CD56+	321	1728	574	538	503	200-400 cells/ul

Red font highlights outside of reference range.
*CMV viremia. All patients were CMV seropositive.

Table 3. Rare variants that were identified and co-segregated in the kindred

	Candidate Disease Alleles	Rare Variant	MAF	Mode of Inheritance
KINDRED A	*IL2RB*	chr22: g.37538526 A>G	0.00001218	Homozygous Recessive
	MRGPRX3	chr11: g.18158885 G>C	0.000198	Homozygous Recessive
	PIDD	chr11: g.801106 G>A	0.00008304	Homozygous Recessive
	ENPP1	chr6: g.132198235 C>G	0	Homozygous Recessive
	ATXN7	chr3: g.63968621 A>T /g.63985157 C>A	0	Compound Heterozygous
KINDRED B	*IL2RB*	chr22: g.37538526 A>G	0.00001218	Homozygous Recessive
	TUBA8	chr22: g.18609211 C>T	0.00018123	Homozygous Recessive
	AIM1	chr6: g.106992691 A>G	0	Homozygous Recessive
	PTAFR	chr1: g.28477001 C>T	0.00090898	Homozygous Recessive
	DCHS1	chr11: g.6661944 C>T	0	Homozygous Recessive
KINDRED C	*IL2RB*	chr22: g.37539634 C>T	0	Homozygous Recessive
	FRMD1*	chr6: g.168479562 G>A	0.02657	Miscalled Variant
KINDRED D	*IL2RB*	chr22: g.37537259 G>A	0	Homozygous Recessive
	NCF4	chr22: g.37267701 G>A	0.001637	Homozygous Recessive
	TTC28	chr22: g.28501414 C>T	0.007219	Homozygous Recessive

MAF= minor allele frequency